

1 Eddy-enhanced primary production sustains heterotrophic microbial 2 activities in the Eastern Tropical North Atlantic

3 Quentin Devresse¹, Kevin W. Becker¹, Arne Bendinger^{1,2}, Johannes Hahn^{1,3}, Anja Engel¹

4 ¹GEOMARHelmholtz Centre for Ocean Research Kiel, Germany,

5 ²Laboratoire d'Etudes en Géophysique et Océanographie Spatiales (LEGOS), Université Toulouse,
6 IRD, CNRS, CNES, UPS, Toulouse, France

7 ³Bundesamt für Seeschifffahrt und Hydrographie, Hamburg, Germany

8

9 Correspondence: Quentin Devresse (qdevresse@geomar.de)

10

11 Abstract

12 Mesoscale eddies modulate the ocean's physical, chemical, and biological properties. In
13 cyclonic eddies (CE), nutrient upwelling can stimulate primary production by phytoplankton.
14 Yet, how this locally enhanced autotrophic production affects heterotrophy and consequently
15 the metabolic balance between the synthesis and the consumption of dissolved organic matter
16 (DOM) remains largely unknown. To fill this gap, we investigated the horizontal and vertical
17 variability of auto- and heterotrophic microbial activity (biomass production and respiration)
18 within a CE that formed off Mauritania and along the ~900 km zonal corridor between
19 Mauritania and the Cape Verde Islands in the eastern tropical North Atlantic (ETNA). Our
20 results show how the physical disturbances caused by the CE affected the biomass distribution
21 of phyto- and bacterioplankton and their metabolic activities.. The injection of nutrients into
22 the sunlit surface resulted in enhanced autotrophic pico- and nanoplankton abundance and
23 generally increased autotrophic activity as indicated by Chlorophyll *a* (Chl-*a*) concentration,
24 primary production (PP) and extracellular release rates. However, the detailed eddy survey
25 also revealed an uneven distribution of these variables with, for example, the highest Chl-*a*
26 concentrations and PP rates occurring near and just beyond the CE's periphery. The
27 heterotrophic bacterial activity was similarly variable. Optode-based community respiration
28 (CR) bacterial respiration (BR) estimates and bacterial biomass production (BP) largely
29 followed the trends of PP and Chl-*a*. Thus, a submesoscale spatial mosaic of heterotrophic
30 bacterial abundance and activities occurred within the CE that was closely related to variability
31 in autotrophic production. Consistent with this, we found a significant positive correlation

32 between concentrations of semi-labile dissolved organic carbon (SL-DOC; here the sum of
33 dissolved hydrolyzable amino acids and dissolved combined carbohydrates) and BR estimates.
34 Extracellular release of carbon as indicated by primary production of dissolved organic carbon
35 (PP_{DOC}) was variable with depth and laterally and not always sufficient to compensate the
36 bacterial carbon demand (BCD: BR+BP) with PP_{DOC} accounting between 28% and 110% of
37 the BCD. Bacterial growth efficiency (BGE: BP/BCD) ranged between 1.7 and 18.2%. We
38 estimated the metabolic state to establish whether the CE was a source or a sink of organic
39 carbon. We showed that the CE carried a strong autotrophic signal in the core (PP/CR>1). Our
40 results suggest that submesoscale (0-10 km) processes lead to highly variable metabolic
41 activities of both photoautotrophic and heterotrophic microorganisms. Overall, we revealed that
42 the CEs not only trap and transport coastal nutrients and organic carbon to the open ocean, but
43 also stimulate phytoplankton growth generating freshly produced organic matter during
44 westward propagation. This drives heterotrophic processes and may contribute to the previously
45 observed net heterotrophy in open Atlantic surface waters.

46

47 1. Introduction

48

49 Mesoscale eddies (10-100 km) are ubiquitous in the ocean affecting upper ocean
50 biogeochemistry and ecology. For example, upwelling of nutrients inside eddies can enhance
51 primary production and carbon export (Cheney and Richardson, 1976; Arístegui et al., 1997).
52 The sense of rotation and their vertical structure classifies cyclonic (CEs), anticyclonic (ACEs;
53 e.g., Chelton et al., 2011) or anticyclonic mode water eddies (ACMEs; D'Asaro 1988). In
54 Eastern Boundary Upwelling Systems (EBUS), eddies typically form by flow separation along
55 slope boundary currents at topographic headlands (D'Asaro, 1988; Molemaker et al., 2015;
56 Thomsen et al., 2016). Eddies have lifespans from days to months and can travel several
57 hundred to thousands of kilometers across ocean basins (Chelton et al., 2011). In the North
58 Atlantic Ocean, eddies generated in the highly productive Canary Upwelling System (CanUS)
59 may laterally propagate to the oligotrophic Subtropical North Atlantic Gyre (SNAG),
60 transporting nutrients and carbon from the coast to the open ocean (McGillicuddy et al., 2003;
61 Karstensen et al., 2015; Schütte et al., 2016). Various studies demonstrated the impact of eddies
62 on primary production (PP) on a global scale. However, the effects of eddies vary regionally,
63 and studies with higher spatial resolution of eddies combined with advances in *in situ*
64 observation, remote sensing and modelling are still needed to better describe the physical and

65 biological properties of the upper ocean. (see review by McGillicuddy, 2016 and references
66 therein). For example, Couespel et al. (2021) performed global warming simulations using a
67 representation of mid-latitude double-gyre circulation. They showed that at the finest model
68 resolution ($1/27^\circ$), eddies can mitigate the decline of primary production (-12 % at $1/27^\circ$ vs. -
69 26 % at 1°). Modeling studies have long urged consideration of the effects of eddies on PP at
70 submesoscale levels (0.1-10 km) to provide more realistic estimates of the oceanic carbon cycle
71 (Lévy et al., 2001). Eddies modulate the mixed layer depth by upwelling (CEs), downwelling
72 (ACEs), or frontogenesis from eddy-eddy interaction, thereby creating spatial variability of
73 nutrient concentration within and around eddies on the submesoscale (see reviews by
74 Mahadevan, 2016 and McGillicuddy, 2016). In addition, the nonlinear response of
75 phytoplankton growth to nutrient availability and advection of phytoplankton by currents makes
76 plankton distribution and community composition highly variable within and around eddies
77 (Lochte and Pfannkuche 1987). As a consequence, the spatial distribution of PP across eddies
78 can be highly variable (e.g., Falkowski et al., 1991; Ewart et al., 2008; Singh et al., 2015).

79 Bacterial activity is directly coupled to PP, as autotrophic cells release their main substrate
80 dissolved organic matter (DOM), . DOM release by phytoplankton mainly occurs via two
81 mechanisms: 1) passive leakage of small molecules by diffusion across the cell membrane and
82 2) active exudation of DOM into the surrounding environment (Engel et al., 2004).
83 Environmental conditions, such as temperature, nutrient availability (e.g., Borchard and Engel,
84 2012) and light conditions (e.g., Cherrier et al., 2015) affect the amount and the elemental
85 stoichiometry of released DOM. Patchiness of phytoplankton primary productivity and nutrient
86 availability within eddies may thus lead to spatial heterogeneity of extracellular release rates
87 (e.g., Lasternas et al., 2013; Rao et al., 2021) and DOM quality (e.g., Wear et al., 2020). DOM
88 quality impacts bacterial biomass production (BP), bacterial respiration (BR), and bacterial
89 growth efficiency (BGE; e.g., Neijssel and de Mattos, 1994; Russell and Cook, 1995; Robinson,
90 2008; Lipson, 2015). BGE is the ratio between BP and the bacterial carbon demand (BCD),
91 which is the sum of respired carbon and carbon incorporated into biomass (BP + BR). Lønborg
92 et al. (2011) observed that BGE decreases with increasing C/N ratio of phytoplankton-derived
93 DOM. BGE is a critical parameter for estimating the amount of consumed organic carbon used
94 to build biomass by heterotrophic bacteria (Anderson and Ducklow 2001). So far, BGE has
95 been reported for ACEs from the Mediterranean Sea (Christaki et al., 2021) but not for CEs and
96 ACMEs. In general, several studies showed a patchy distribution of bacterial abundance, BP
97 (Ewart et al., 2008; Baltar et al., 2010), BR (Mouriño-Carballido, 2009; Jiao et al., 2014),

98 community respiration (CR; Mouriño-Carballido and McGillicuddy, 2006; Mouriño-
99 Carballido, 2009), and of the metabolic balance between the production and consumption of
100 organic matter (Maixandeu et al., 2005; Ewart et al., 2008; Mouriño-Carballido and
101 McGillicuddy, 2006; Mouriño-Carballido, 2009) within eddies. Yet, insights into the
102 distribution of phytoplankton and their activities within mesoscale eddies are limited due to
103 insufficient fine-scale vertical and horizontal resolution studies to adequately describe these
104 distributions. Thus, data on eddy-induced changes in primary production, extracellular release
105 and semi-labile DOM concentration, and the responses of heterotrophic microbial metabolic
106 activities are scarce. Understanding how eddies modulate microbial activities will enhance our
107 knowledge about the fate of organic carbon and the overall CO₂ source/sink function in the
108 ocean, particularly in EBUS, where eddy generation is high (Pegliasco et al., 2015).

109 Here, we studied the impact of a CE on microbial carbon cycling along a 900 km zonal corridor
110 of the westward propagating eddies between the Cape Verde Islands and the Mauritania
111 Upwelling System (13-20 °N), a sub-region of the CanUS (13-33 °N, Arístegui et al., 2009).
112 About 146 ± 44 eddies with a lifetime of more than 7 days are generated per year in this region
113 (Schütte et al., 2016). Along this corridor, a CE was sampled at high spatial resolution to resolve
114 the heterogeneity of microbial processes at the submesoscale. We determined phytoplankton
115 (<20 µm) cell abundance, primary production, and extracellular release and linked those
116 measurements of autotrophic activity to semi-labile DOM concentration and heterotrophic
117 bacterial activity. Our study provides new insights into 1) microbial carbon cycling and 2)
118 factors controlling microbial metabolic activities within and around CE formed in EBUS.

119

120 2. Materials and Methods

121

122 2.1 Study area and eddy characterization

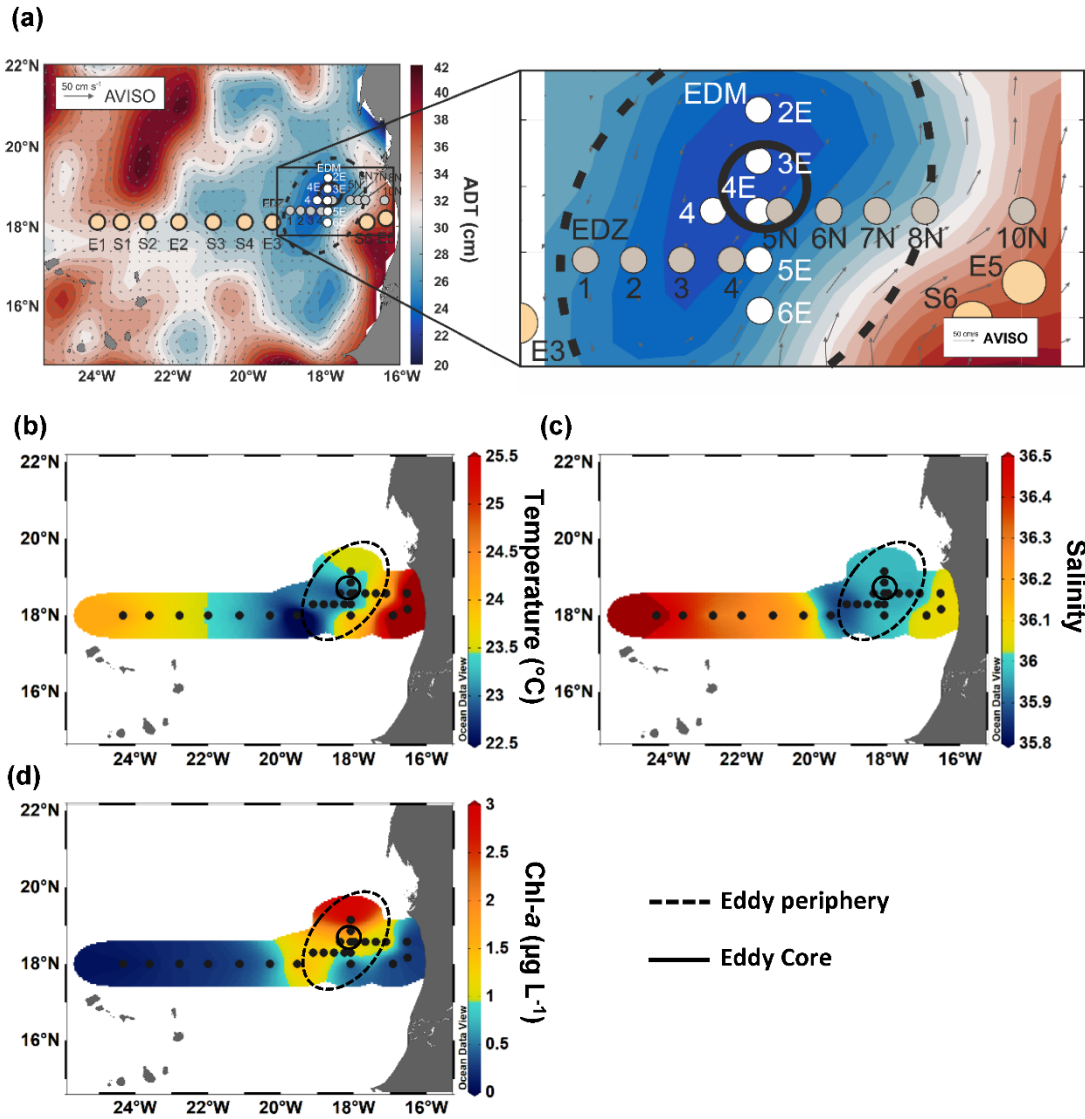
123

124 Sampling was conducted in the ETNA between the Cape Verde archipelago and the
125 Mauritanian coast during cruise M156 (July 3rd to August 1st, 2019. Figure 1A) on the R/V
126 *Meteor*. Samples were collected during the relaxation period, which is typically from May to
127 July following the upwelling season (January to March; Lathuilière et al., 2008). A CE was
128 sampled at high spatial resolution along two zonal transects (from 19.1 °W to 18.2 °W at 18.3
129 °N and from 18.5 °W to 17.1 °W at 18.6 °N) and one meridional transect (from 19.4 °N to 18

130 °N at 18.4 °W to 18.1 °W). The zonal transect slightly shifted east/west of the eddy core
131 position. The reason for that was the deformed eddy shape (see Fig. 1A), which made it
132 challenging to identify the center of the eddy and required rerouting of the ship's track during
133 the survey. In addition, we sampled water along an 18 °N transect, a typical coast to open ocean
134 trajectory of eddies in this region (Schütte et al., 2016). Salinity, temperature, depth, and O₂
135 concentration were determined using a Seabird 911 plus CTD system equipped with two
136 independently working sets of temperature-conductivity-oxygen sensors. The oxygen sensor
137 was calibrated against discrete water samples using the Winkler method (Strickland and
138 Parsons, 1968; Wilhelm, 1888). Seawater samples were collected using 10 L Niskin bottles
139 attached to the CTD Rosette. A total of 25 stations (SI Table S1) were sampled, 14 of them
140 inside or in the vicinity of the CE. Sampling was conducted in the epipelagic layer (0-200 m),
141 including samples from the surface mixed layer, the Chl-*a* maximum, and the shallow oxygen
142 minimum zone (OMZ; <50 μmol kg⁻¹ between 0-200 m depth) when present.

143 Sea surface height (SSH) and Acoustic Doppler Current Profiler (ADCP) velocity data (SI Fig.
144 1) characterized the eddy as a CE. Based on the Angular Momentum Eddy Detection and
145 Tracking Algorithm (AMEDA; Le Vu et al., 2018), the eddy was estimated to be 1.5 months
146 old. The center of the eddy and the core radius were determined using ADCP reconstructions
147 assuming an axis-symmetric vortex. (SI Fig. 1). On July 22nd 2019, the eddy center was located
148 at 18.69 °N, 18.05 °W, with a core radius of 40.5 ± 5.7 km. The mean azimuthal velocity in the
149 CE was 19.9 ± 0.7 cm s⁻¹ and the absolute dynamic topography associated with the CE core
150 was ~23 cm on July 23rd 2019. However, as the eddy shape was deformed, ADCP
151 reconstruction did not constrain well the physical border of the eddy (SI Fig. S1). Therefore,
152 we combined sea surface temperature (23.44 ± 0.47 °C), salinity (39.95 ± 0.04) and Chl-*a* (1.35
153 ± 0.73 μg L⁻¹) data to approximate the area influenced by the eddy (Fig. 1b,c,d). We classified
154 stations into 'core' and 'periphery' of the eddy. Stations that were outside and westward of the
155 eddy influence were referred to as 'open ocean' and those close to the coast as 'coastal'. Just
156 beyond the eddy periphery, at St. E3, a front was observed with surface temperature and salinity
157 (not compensated by density) different from the adjacent stations (Fig. 1b). Hence, we referred
158 to that station as 'Frontal Zone'. The classification of stations is thoroughly discussed in the
159 supplementary information (SI), and the sampling time, location, and distance from the eddy
160 center are given in SI Table S1.

161



162

163

164 Figure 1: Sampling stations during RV *Meteor* cruise M156 including zoom in into the eddy (a),
 165 temperature at 5 m depth (b), salinity at 5 m depth (c), and chlorophyll *a* at 5 m depth (d). The
 166 background in (a) shows the variations in Absolute Dynamic Topography (ADT) obtained from
 167 www.aviso.altimetry.fr. The direction and speed of surface water geostrophic currents are shown as
 168 arrows. The solid circle in (a) – (d) indicates the core of the eddy and the dashed circle outlines the
 169 periphery.

170

171 2.2 Chemical analyses

172 Nutrient concentrations were determined at selected stations (SI Table S1). Nutrients were
 173 measured onboard from duplicate unfiltered seawater samples (11 mL). Ammonium (NH_4^+)
 174 was analyzed after Solórzano (1969) and phosphate (PO_4), nitrate (NO_3^-), nitrite (NO_2^-), and

175 silicate (Si(OH)_4) were measured photometrically with continuous-flow analysis on an auto-
176 analyzer (QuAatro; Seal Analytical) after Grasshoff et al., (1999). Detection limits for NH_4^+ ,
177 PO_4 , NO_3 , NO_2 , and Si(OH)_4 were 0.1, 0.02, 0.1, 0.02, and $0.2 \mu\text{mol L}^{-1}$, respectively. Dissolved
178 inorganic nitrogen (DIN) was calculated as the sum of NH_4^+ , NO_3^- , and NO_2^- .

179 To estimate the fraction of semi-labile dissolved organic carbon (SL-DOC), we determined
180 high-molecular-weight ($\text{HMW} > 1 \text{ kDa}$) dissolved combined carbohydrates (dCCHO) and
181 dissolved hydrolysable amino acids (dHAA) as the main biochemical components of DOM
182 (Carlson, 2002). For dCCHO analysis, duplicate samples (20 mL) were filtered through 0.45
183 μm Acrodisk filters, collected in combusted glass vials (8 h, $450 \text{ }^\circ\text{C}$) and frozen ($-20 \text{ }^\circ\text{C}$) until
184 analysis after Engel and Händel (2011) with a detection limit of $1 \mu\text{g L}^{-1}$. The analysis detected
185 11 monomers: arabinose, fucose, galactose, galactosamine, galacturonic acid, glucosamine,
186 glucose, glucuronic acid, rhamnose, co-elute mannose, and xylose. For dHAA analysis,
187 duplicate samples (4 mL) were filtered through $0.45 \mu\text{m}$ Acrodisk filters, collected in
188 combusted glass vials (8 h, $450 \text{ }^\circ\text{C}$), and frozen ($-20 \text{ }^\circ\text{C}$) until analysis. dHAA were measured
189 with ortho- phthaldialdehyde derivatization by high-performance liquid chromatography
190 (HPLC; Agilent Technologies, USA) equipped with a C_{18} column (Phenomenex, USA)
191 (Lindroth and Mopper, 1979; Dittmar et al., 2009). The analysis classified 13 monomers with
192 a precision $< 5 \%$ and a detection limit of 2 nmol L^{-1} : alanine, arginine, aspartic acid, isoleucine,
193 glutamic acid, glycine, leucine, phenylalanine, serine, threonine, tyrosine, valine; and γ -
194 aminobutyric acid (GABA). The calculations for the carbon content of dCCHO and dHAA were
195 based on carbon atoms contained in the identified monomers. The sum of dCCHO and dHAA
196 carbon content is referred to as SL-DOC.

197 For Chl-*a*, 1 L seawater samples were filtered onto 25 mm GF/F filters ($0.7 \mu\text{m}$ pore size,
198 Whatman, GE Healthcare Life Sciences, UK) and subsequently frozen ($-20 \text{ }^\circ\text{C}$) until extraction
199 using 90% acetone for photometric analyses (Turner Designs, USA) slightly modified after
200 Evans et al., (1987).

201 Bacteria were quantified using a flow cytometer (FACSCalibur, Becton Dickinson, Oxford,
202 UK). Seawater samples (1.7 mL) were fixed with $85 \mu\text{L}$ glutaraldehyde (1% final
203 concentration) and stored at $-80 \text{ }^\circ\text{C}$ until analysis. Samples were stained with SYBR Green I
204 (molecular probes) and enumerated with a laser emitting at 488 nm and detected by their
205 signature in a plot of side scatter (SSC) versus green fluorescence (FL1). Heterotrophic bacteria
206 were distinguished from photosynthetic bacteria (*Prochlorococcus* and *Synechococcus*) by their
207 signature in a plot of red fluorescence (FL2) versus green fluorescence (FL1). Yellow-green

208 latex beads (1 μm , Polysciences) were used as an internal standard (Gasol and del Giorgio,
209 2000). Cell counts were determined with the CellQuest software (Becton Dickinson). For
210 autotrophic pico and nanoplankton $<20 \mu\text{m}$, 2 mL samples were fixed with formaldehyde (1 %
211 final concentration) and stored frozen ($-80 \text{ }^\circ\text{C}$) until analysis. Red and orange autofluorescence
212 was used to identify Chl-*a* and phycoerythrin cells. Cell counts were determined with CellQuest
213 software (Becton Dickinson); picoplankton and nanoplankton populations containing Chl-*a*
214 and/or phycoerythrin (i.e., *Synechococcus*) were identified and enumerated. We converted the
215 cell abundance of the different autotrophic pico- and nanoplankton populations into biomass
216 assuming 43 fg C cell⁻¹ for *Prochlorococcus*, 120 fg C cell⁻¹ for *Synechococcus*, 500 fg C cell⁻¹
217 for eukaryotic picoplankton and, 3.100 fg C cell⁻¹ for eukaryotic nanoplankton after
218 Hernández-Hernández et al. (2020). We report the autotrophic pico- and nanoplankton biomass
219 as the sum of eukaryotic pico- and nanoplankton and cyanobacteria (*Prochlorococcus* and
220 *Synechococcus*) biomass. The abundance of eukaryotic pico- and nanoplankton and
221 cyanobacteria (*Prochlorococcus* and *Synechococcus*) can be found in the SI (Table S2).

222

223 2.3 Microbial activities

224

225 Primary production (PP) was determined from ¹⁴C incorporation according to Steemann
226 Nielsen (1952) and Gargas (1975). Polycarbonate bottles (Nunc EasYFlask, 75 cm²) were filled
227 with 260 mL prefiltered (mesh size of 200 μm) sample and spiked with 50 μL of a $\sim 11 \mu\text{Ci}$
228 $\text{NaH}^{14}\text{CO}_3^-$ solution (Perkin Elmer, Norway). 200 μL were removed immediately after spiking
229 and transferred to a 5 mL scintillation vial for determination of added activity. Then, 50 μL of
230 2N NaOH and 4 mL scintillation cocktail (Ultima Gold AB) were added. Duplicate samples
231 from the top three depths at selected stations (SI Table S1) were incubated in 12 h light and 12
232 h dark at 22 $^\circ\text{C}$, which was the average temperature of the upper 100 m depth ($22 \pm 3^\circ\text{C}$) along
233 the transect. The incubator was set to reproduce three light levels: 1200-1400; 350 and 5 μE ,
234 with high values representing surface irradiance at the time of sampling. The incubation length
235 was chosen for two reasons. First, we expected low productivity of the open ocean
236 phytoplankton community due to low biomass and low nutrient concentrations at the start of
237 the incubation. Under these conditions, short-term incubations of only a few hours may
238 underestimate PP because carbon assimilation by algal cells may be too low to discriminate
239 against ¹⁴C adsorption as determined in blank dark incubation (Engel et al., 2013). Moreover,
240 the release of freshly assimilated carbon into the DOM pool has a time scale of several hours

241 because of the equilibration of the tracer and because metabolic processes of organic carbon
 242 exudation follow those of carbon fixation inside the cell (Engel et al., 2013). Incubations were
 243 stopped by filtration of a 70 mL sub-sample onto 0.4 μm polycarbonate filters (Nuclepore).
 244 Particulate primary production (PP_{POC}) was determined from material collected on the filter,
 245 while the filtrate was used to determine dissolved primary production (PP_{DOC}). All filters were
 246 rinsed with 10 mL sterile filtered ($<0.2 \mu\text{m}$) seawater, and then acidified with 250 μL 2N HCl
 247 to remove inorganic carbon (Descy et al., 2002). Filters were transferred into 5 mL scintillation
 248 vials, and 4 mL scintillation cocktail (Ultima Gold AB) was added. To determine PP_{DOC} , 4 mL
 249 of filtrate were transferred to 20 mL scintillation vials and acidified with 100 μL 1N HCl.
 250 Scintillation vials were left open in the fume hood for 14 hours to remove inorganic carbon.
 251 Then, 100 μL of 2N NaOH and 15 mL scintillation cocktail were added. All samples were
 252 counted the following day in a liquid scintillation analyzer (Packard Tri-Carb, model 1900 A).

253 Primary production (PP) of organic carbon was calculated according to Gargas (1975):

254

$$255 \quad \text{PP } (\mu\text{mol C L}^{-1} \text{ d}^{-1}) = \frac{a_2 \times \text{DI}^{12}\text{C} \times 1.05 \times k_1 \times k_2}{a_1} \quad (\text{Eq.1})$$

256

257 where a_1 and a_2 are the activities (DPM) (disintegrations per minute) of the added solution
 258 and the sample corrected for dark sample, respectively, and DI^{12}C is the concentration (μmol
 259 L^{-1}) of dissolved inorganic carbon (DIC) in the sample. DIC concentration was calculated from
 260 total alkalinity using the R package seacarb (Gattuso et al., 2020). Total alkalinity of the
 261 seawater was acquired through the open-cell titration method (Dickson et al., 2007). The value
 262 1.05 is a correction factor for the discrimination between ^{12}C and ^{14}C , as the uptake of the ^{14}C
 263 isotope is 5% slower than the uptake of ^{12}C , k_1 is a correction factor for subsampling (bottle
 264 volume/filtered volume) and k_2 is the incubation time (d^{-1}). Total primary production (PP_{TOT} ;
 265 $\mu\text{mol C L}^{-1} \text{ d}^{-1}$) was derived from the sum of PP_{POC} and PP_{DOC} according to:

266

$$267 \quad \text{PP}_{\text{TOT}} = \text{PP}_{\text{POC}} + \text{PP}_{\text{DOC}} \quad (\text{Eq.2})$$

268

269 The percentage of extracellular release (PER; %) was calculated as:

$$270 \quad \text{PER} = \left(\frac{\text{PP}_{\text{DOC}}}{\text{PP}_{\text{TOT}}} \right) \times 100 \quad (\text{Eq.3})$$

271

272 Bacterial biomass production rates (BP) were measured through the incorporation of labeled
273 leucine (^3H) (specific activity 100 Ci mmol^{-1} , Biotrend) using the microcentrifuge method
274 (Kirchman et al., 1985; Smith and Azam, 1992). Duplicate samples and one killed control (1.5
275 mL each) were labeled using ^3H -leucine at a final concentration of 20 nmol L^{-1} . BP was
276 determined down to 800 m depth and, for practical reasons, we chose an incubation temperature
277 of $14 \text{ }^\circ\text{C}$ as an average over this depth interval. However, in this paper, only data from the top
278 100 m depth are shown and BP rates were corrected for the difference between incubation and
279 *in situ* temperature (Eq. 4). All samples were incubated for 6 h in the dark with headspace.
280 Controls were poisoned with trichloroacetic acid. All Samples were measured on board with a
281 liquid scintillation analyzer (Packard Tri-Carb, model 1900 A). ^3H -leucine uptake was
282 converted to carbon units by applying a conversion factor of $1.55 \text{ kg C mol}^{-1}$ leucine (Simon
283 and Azam, 1989).

284 BP rates from incubations at $14 \text{ }^\circ\text{C}$ were converted to BP rates at $22 \text{ }^\circ\text{C}$ following the equation
285 from López-Urrutia and Morán (2007):

286
$$BP_{22^\circ\text{C}} = BP_{14^\circ\text{C}} \times 1.906 \quad (\text{Eq. 4})$$

287 Community respiration rates (CR) were estimated from quadruplicate incubations by measuring
288 changes of dissolved oxygen over 24-36 hours at the same temperature as used for BP ($14 \text{ }^\circ\text{C}$)
289 using optode spot mini sensors (PreSens PSt3; Precision Sensing GmbH, Regensburg,
290 Germany). The detection limit (DL) for CR was $0.55 \text{ } \mu\text{mol O}_2 \text{ L}^{-1} \text{ d}^{-1}$.

291 CR at 22°C was estimated using the extrapolation from Regaudie-De-Gioux and Duarte (2012):

292
$$CR_{22^\circ\text{C}} = CR_{14^\circ\text{C}} \times 2.011 - 0.013 \quad (\text{Eq. 5})$$

293 $CR_{22^\circ\text{C}}$ was converted into bacterial respiration ($BR_{22^\circ\text{C}}$) after Aranguren-Gassis et al. (2012):

294
$$BR_{22^\circ\text{C}} = 0.30 \times CR_{22^\circ\text{C}}^{1.22} - 0.013 \quad (\text{Eq. 6})$$

295 A respiratory quotient of 1 was used to convert oxygen consumption into carbon respiration
296 (del Giorgio and Cole 1998).

297 We estimated the bacterial carbon demand (BCD) as follows:

298
$$BCD = BP + BR \quad (\text{Eq. 7})$$

299 Bacterial growth efficiency (BGE) was calculated from BP and BCD:

300
$$BGE = \frac{BP}{BCD} \quad (\text{Eq. 8})$$

301 Detailed information on procedures and calculations of microbial activities are provided in the
302 SI.

303
304 **2.4 Data analysis**

305 Statistical analyses and calculations were conducted using the software R (v4.0.3) in R studio
306 (v1.1.414; Ihaka and Gentleman 1996). Analysis of variances (ANOVA) and Tukey test, were
307 performed on the different parameters by grouping the station by their position (SI Table **S1**).
308 Seawater density was calculated using R package oce v1.3.0 (Kelley, 2018) and the mixed layer
309 maximum depth was determined as the depth at which a change from the surface density of
310 0.125 kg m^{-3} has occurred (Levitus, 1982). Erroneous estimates of mixed layer maximum depth
311 have been corrected manually on five profiles. Other R packages used in this study include
312 corrplot v0.84 (Dray, 2008) and ggplot2 v3.3.3 (Wickham, 2016). Section plots were made
313 using Ocean Data View v5.6.2 (Schlitzer, 2020). Depth integrated values were calculated using
314 the midpoint rule.

315 **3. Results**

316
317 **3.1 Hydrographic conditions**

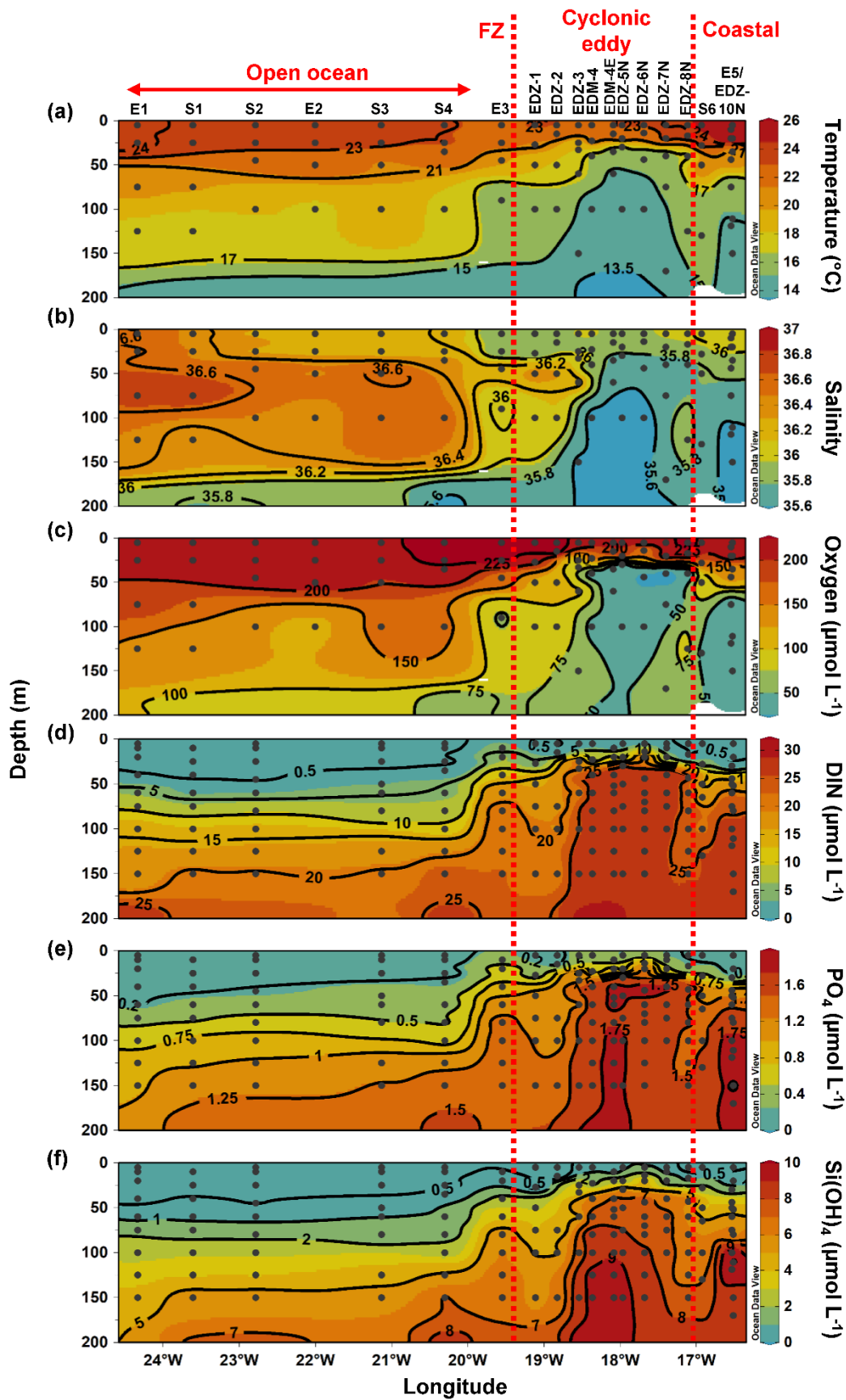
318 Along the zonal transect, open ocean waters (from 20 to 24.5 °W) had a temperature range of
319 13.45-24.2 °C and a salinity between 35.55-36.79 in the upper 200 m depth (Fig. **2a** and **b**).
320 The average mixed layer depth was 35 ± 7 m (Fig. **3a**; SI Table **S1**). Oxygen concentrations
321 (Fig. **2c**) decreased with depth while nutrient concentrations increased (Fig. **2d-e**). Nutrients
322 were depleted (<0.5 , <0.2 , and $<0.5 \mu\text{mol L}^{-1}$ for DIN, PO_4 , $\text{Si}(\text{OH})_4$, respectively) in the mixed
323 layer.

324 At the coastal stations (16.51 to 16.92 °W), the temperature had a range of 14.6-26.1 °C and a
325 salinity between 35.53 and 36.08 in the upper 200 m depth (Fig. **2a** and **b**). Here, the mixed
326 layer was shallower than in the open ocean but not significantly (Tukey, $p>0.05$), with an
327 average depth of 24.5 ± 9 m (Fig. **3a**; SI Table **S1**). Oxygen was decreasing with depth and a
328 shallow oxygen minimum zone (OMZ; $<50 \mu\text{mol kg}^{-1}$) was detected between 80 m and 200 m
329 depth (Fig. **2c**). Nutrients (Fig. **2d-e**) were depleted at the surface (5 m depth), while the deeper
330 coastal waters (~ 80 to 200 m depth) were colder and richer in nutrients than the open ocean

331 waters, with on average 3.4-fold higher nutrient concentrations (DIN, PO₄, Si(OH)₄) when
332 integrated over 100 m depth (data not shown).

333 In the CE ('periphery' and 'core'), waters had a temperature range of 13.2-24.2 °C and a salinity
334 between 35.48 and 36.36 in the upper 200 m depth (Fig. **2a** and **b**). A compression of isopycnals
335 with a strong doming of the isotherms, isohalines, and nutrients isolines was observed (Fig. **2a-**
336 **b, d-f**). A shallow OMZ was detected from ~30 m to ~100 m depth with the lowest oxygen
337 concentration (<10 μmol kg⁻¹) between 30-40 m. The mixed layer was significantly shallower
338 (Tukey, *p*<0.05) in the CE periphery and in the CE core than in the open ocean with an average
339 of 15 ± 6 m and 20 ± 2 m depth respectively (Fig. **3a**). At the surface (5 m depth), nutrients
340 were depleted (<0.5, <0.2 and <0.5 μmol L⁻¹ for DIN, PO₄, Si(OH)₄, respectively) only in the
341 most eastern (17.11 °W, 18 °N) and western (18.83-19.11 °W, 18.58 °N) part of the CE
342 periphery (Fig. **2d-f**). In the core, nutrient concentrations were also lowest in the surface water,
343 but richer in nutrients than in the ambient waters.

344 The Frontal Zone station E3 (19.55 °W) was distinct from the adjacent stations with respect to
345 surface temperature (1 °C colder, Fig **2a**). A doming of the nutrients isolines was observed
346 (Fig.**2d-f**) and nutrient concentrations integrated over 100 m depth at St. E3 were ~3 fold higher
347 than at the open ocean S4 (20.3 °W) and ~1.2 fold higher than at the CE periphery St. EDZ-1
348 (19.11 °W).

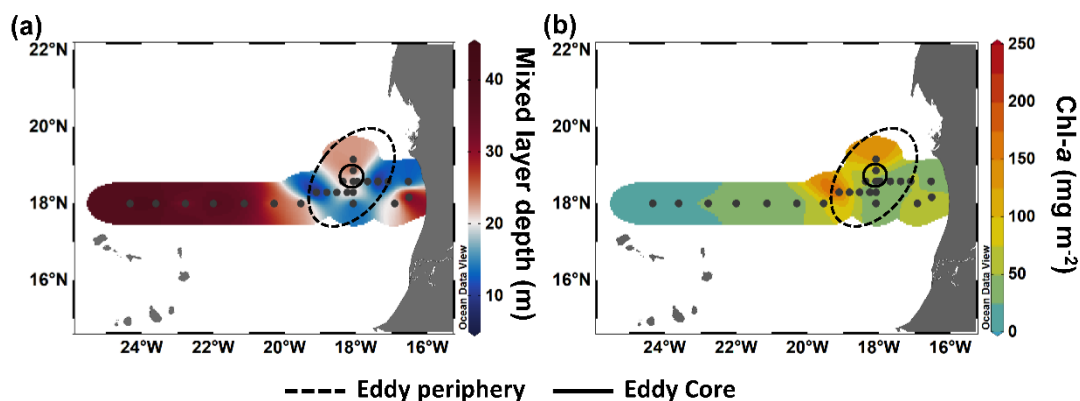


349

350 Figure 2: Epipelagic distribution (0-200 m) of temperature (a), salinity (b), oxygen (c), total inorganic
 351 nitrogen (DIN) (d), phosphate (PO_4) (e), and silicate (Si(OH)_4) (f). Red dashed lines show the western
 352 and eastern boundary of the cyclonic eddy periphery, respectively. FZ refers to Frontal Zone.

3.2 Chlorophyll-*a* and primary production

In order to compare stations along the zonal transect and within the eddy, data were integrated over the water column (0-100 m depth). Along the zonal transect, depth-integrated Chl-*a* concentration ranged between 11.7 and 58.7 mg m⁻² and decreased from the coastal to the open ocean stations (Table 1; Fig. 3b). Depth-distribution showed a Chl-*a* maximum in the open ocean around ~75 m from 23.61 to 24.33 °W and around ~50 m from 22.78 to 20.3 °W, up to 0.68 μg L⁻¹ (Fig. 4a). At the coastal stations, the Chl-*a* maximum was found between 30-40 m depth with values up to 0.96 μg L⁻¹. Integrated biomass of autotrophic pico- and nanoplankton (Table 1) ranged between 1.6 and 7.8 and between 3.6 and 6.1 g C m⁻² in the open ocean and at the coastal stations, respectively. In the open ocean waters, the depth distribution of autotrophic pico- and nanoplankton biomass (Fig. 4b) showed a gradient from west to east with a concentration maximum at ~75 m from 23.61 to 24.33 °W, a concentrations maximum at ~50 m from 22 to 22.78 °W, and a concentrations maximum between 5-25 m from 21.13 to 20.3 °W. Concentrations reached up to 166 μg C L⁻¹. At the coastal stations, the maximum autotrophic pico- and nanoplankton biomass was found between 30-40 m depth with values up to 117 μg C L⁻¹. Both Chl-*a* concentration and autotrophic pico- and nanoplankton biomass did not vary significantly between the open ocean and the coastal stations (Tukey, *p*>0.05). Integrated total and dissolved primary production (PP_{TOT}; PP_{DOC}; Table 1) remained fairly constant with ranges of 101-137 and 42.8-78 mmol C m⁻² d⁻¹, respectively, at the coastal and the open ocean stations. An exception was the station furthest offshore (24.33 °W), where rates decreased sharply to 25.8 mmol C m⁻² d⁻¹ for PP_{TOT} and to 12.3 mmol C m⁻² d⁻¹ for PP_{DOC}. The integrated percentage of extracellular release (PER; Table 1) ranged between 42.3 and 67.5%. PP_{DOC} and PER did not vary significantly between the open ocean and the coastal stations (Tukey, *p*>0.05). PP_{TOT} and PP_{DOC} decreased with depth except for station E2 (Fig. 4c), while PER increased (Fig. 4d).



378

379 Figure 3: Spatial distribution of maximum mixed layer depth (**a**) and integrated chlorophyll *a* (Chl-*a*)
380 over 100 m depth (**b**) during M156.

381 In the CE (core and periphery) and at the Frontal Zone, integrated Chl-*a* concentration ranged
382 from 17.2 to 225 mg m⁻² (Table 1). The Chl-*a* distribution (Fig. 3a) showed a clear spatial
383 separation with the highest values (98.7-225 mg m⁻²) in the western and northern (148 mg m⁻²)
384 parts of the CE and lowest values (26.8-37.5 mg m⁻²) in the southern and eastern part. Depth
385 distribution of Chl-*a* concentration also differed across the eddy, with values >0.5 µg L⁻¹
386 reaching down to 45 m depth at the Frontal Zone and the western part of the CE and down to
387 30 m depth in the eastern part of the CE (Fig. 4a). Highest concentrations were detected in the
388 western part of the eddy with 8.7 µg L⁻¹ at station EDZ-1 at 27 m. Within the upper 30 m, Chl-
389 *a* concentration within the CE was significantly higher than at the open ocean and the coastal
390 stations (ANOVA, *p*<0.05). Integrated autotrophic pico- and nanoplankton biomass ranged
391 between 0.3 and 4.7 g C m⁻² in the CE (Table 1). Depth distribution of autotrophic pico-
392 nanoplankton biomass (Fig. 4b) showed low biomass in the upper 40 m (<25 µg C L⁻¹) from
393 18.83 to 19.11 °W. In contrast, higher biomass (>25 µg C L⁻¹) occurred in the more eastern
394 stations of the CE (17.11 to 18.54 °W) and westwards from the Frontal Zone (19.55 °W). In the
395 eddy, autotrophic pico- and nanoplankton biomass reached higher concentrations mainly within
396 the upper 40 m, with values up to 191 µg C L⁻¹. Depth-integrated PP_{TOT} and PP_{DOC} rates were
397 significantly higher in the CE and at the Frontal Zone than in the open ocean and the coastal
398 stations (Tukey, *p*<0.05) with values ranging from 245 to 687 mmol C m⁻² d⁻¹ and from 95.9 to
399 238 mmol C m⁻² d⁻¹, respectively (Table 1). PP_{TOT} rates (Fig. 4c; Table 2) were fairly constant
400 across the CE's surface (5 m depth), ranging between 11.2 and 13.7 µmol C L⁻¹ d⁻¹, but varied
401 strongly between 15-40 m depth (0.2-14.5 µmol C L⁻¹ d⁻¹). The highest PP_{TOT} rates were found
402 in the Frontal Zone with up to 25.0 µmol C L⁻¹ d⁻¹ at the surface. The range of PP_{DOC} rates
403 (Table 2; Fig. 4d) was larger in the CE (0.2-4.9 µmol C L⁻¹ d⁻¹) and the Frontal Zone (0.7-7.8
404 µmol C L⁻¹ d⁻¹) than in the open ocean and at the coastal stations. Integrated PER had a range
405 of 29.4-40.8 % (Table 1). Compared to open ocean and coastal stations, a slightly lower PER
406 was observed within the upper 40 m (Fig. 4e) for the CE and Frontal Zone.

407

408

409

410

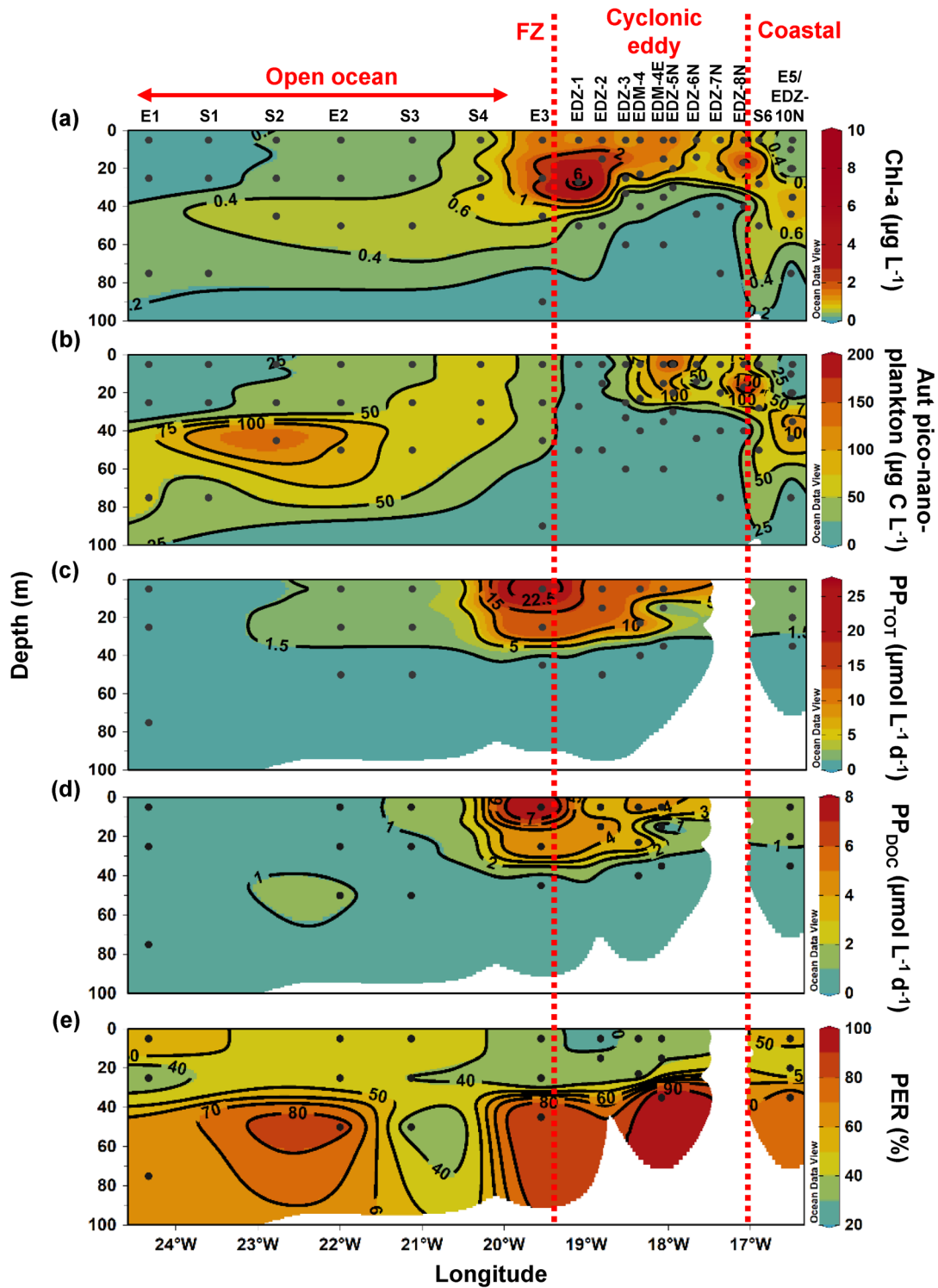
411 Table 1: Chlorophyll *a* (Chl-*a*) and abundance, biomass and activity of phyto- and bacterial plankton,
 412 integrated over the upper 100 m depth. ‘-’ indicate that the variable was not measured. Sampling date,
 413 time and depth can be found in SI Table S1.

Location	Station	Chl- <i>a</i> (mg m ⁻²)	Autpico- nanoPl (g C m ⁻²)	PP _{DOC} (mmol C m ⁻² d ⁻¹)	PP _{TOT} (mmol C m ⁻² d ⁻¹)	PER (%)	HB (10 ¹⁵ cell m ⁻²)	CR (mmol C m ⁻² d ⁻¹)	BR (mmol C m ⁻² d ⁻¹)	BP (mmol C m ⁻² d ⁻¹)
Coastal	E5	54.5	6.1	75.2	137	54.9	14.7	99.6	32	5.6
	EDZ-10N	36.8	3.6	-	-	-	13.8	-	-	7.9
	AZM-3	58.7	5.3	-	-	-	12.9	-	-	10.8
Eddy Periphery	EDZ-8N	61.5	4.7	-	-	-	10.7	-	-	15.6
	EDZ-7N	26.8	1.6	-	-	-	9.4	-	-	10.8
	EDZ-6N	27.9	1.2	-	-	-	9.1	-	-	7.5
Eddy Core	EDZ-5N	39.2	4.1	-	-	-	14.5	154	59.1	9.0
	EDM-4E	46.0	3.3	95.9	245	39.2	15.2	135	60.8	8.6
	EDM-3E	77.5	3.2	-	-	-	15.3	-	-	16.4
	EDM-4	63.8	3.3	141	380	37.2	19.4	275	127	12.2
Eddy Periphery	EDM-6E	35.7	3.6	117	288	40.8	23.7	-	-	13.0
	EDM-5E	35.2	1.6	-	-	-	11.8	-	-	9.0
	EDM-2E	148	1.7	-	-	-	20.8	-	-	21.8
	EDZ-4	47.8	1.0	-	-	-	14.4	-	-	12.0
	EDZ-3	17.2	0.3	-	-	-	9.6	-	-	5.6
	EDZ-2	98.7	0.7	131	445	29.4	8.2	592	320	15.5
EDZ-1	225	0.6	-	-	-	13.7	-	-	36.7	
Frontal Zone	E3	72.1	2.4	238	687	34.6	12.9	529	257	14.7
Open ocean	S4	40.2	4.5	-	-	-	16.9	-	-	8.2
	S3	30.7	4.0	42.8	101	42.3	14.5	346	148	5.0
	E2	22.3	4.4	78.0	116	67.5	12.2	387	168	3.9
	S2	34.1	7.8	-	-	-	13.9	-	-	4.4
	S1	12.2	1.6	-	-	-	5.4	-	-	1.4
	E1	11.7	2.3	12.3	25.8	47.6	6.7	19.7	6.3	1.6

414

415

416



418 Figure 4: Depth distribution of phytoplankton biomass and activity from the surface to 100 m.
 419 Chlorophyll *a* (Chl-*a*; **a**), Autotrophic pico- and nanoplankton biomass (Aut pico-nanoplankton; **b**), total
 420 primary production (PP_{TOT} ; **c**), dissolved primary production (PP_{DOC} ; **d**) and percentage of extracellular
 421 release (PER; **e**). Red dashed lines show the western and eastern boundary of the cyclonic eddy
 422 periphery, respectively. FZ refers to Frontal Zone.

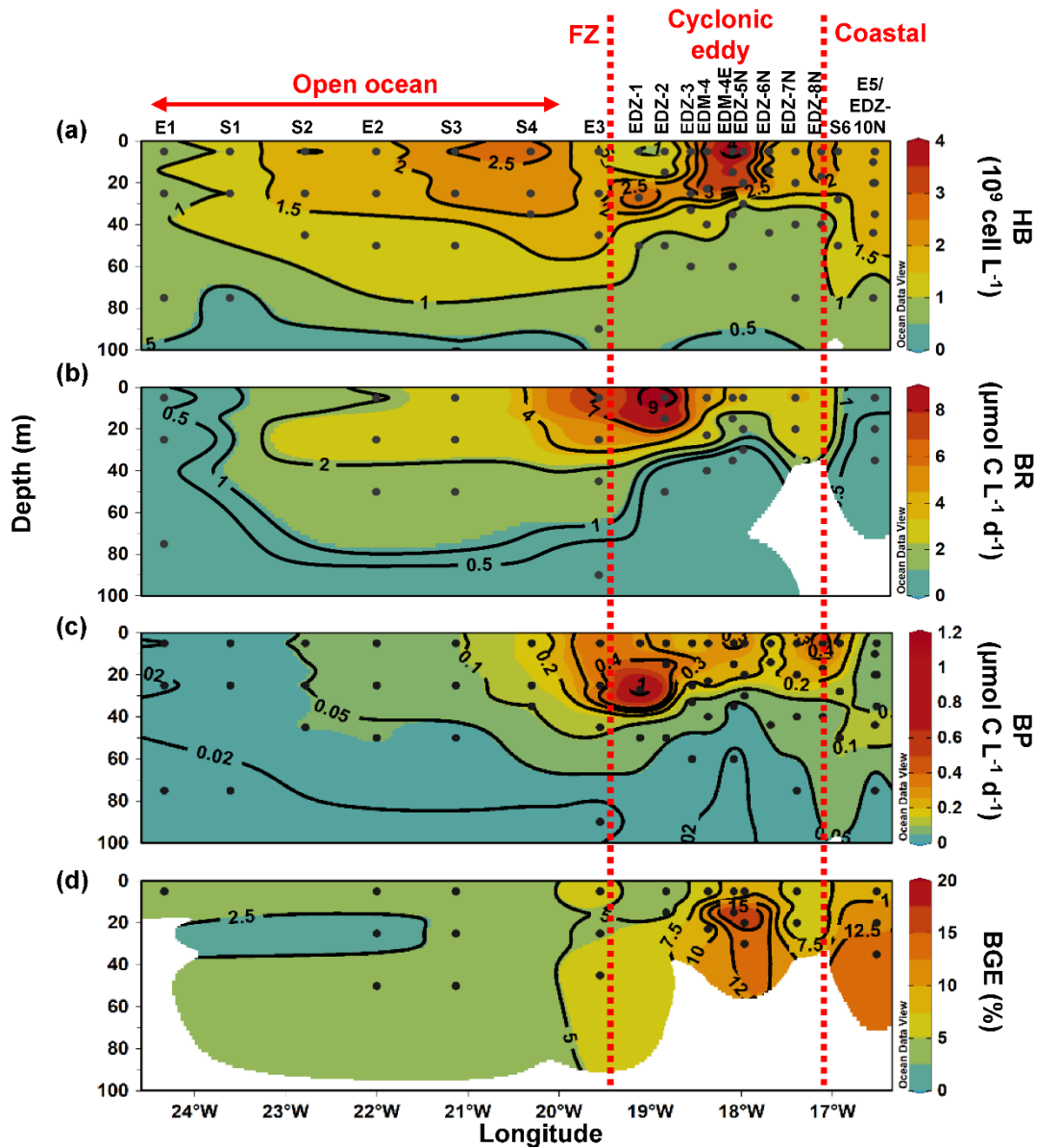
423

424 3.3 Bacterial abundance and activities

425 Heterotrophic bacterial abundance decreased with depth and was highest in the upper 50 m at
426 all stations (Fig. 5a). At the coastal and open ocean stations, integrated (0-100 m) heterotrophic
427 bacteria abundance ranged between 12.9-14.7 and 5.4-16.9 $\times 10^{15}$ cells m^{-2} , respectively (Table
428 1). No significant differences in heterotrophic bacterial abundance were observed between the
429 open ocean and coastal stations (Tukey, $p > 0.05$). In the open ocean waters, the lowest integrated
430 BR and CR rates were observed at the station furthest offshore (E1), with 6.3 and 19.7 mmol C
431 $m^{-2} d^{-1}$, respectively (Table 1). At the other open ocean stations, integrated BR and CR rates
432 ranged between 148-168 mmol C $m^{-2} d^{-1}$ and 346-348 mmol C $m^{-2} d^{-1}$, respectively, which was
433 higher than at the coastal station with BR rates of 32 mmol C $m^{-2} d^{-1}$ and CR rates of 98 mmol
434 C $m^{-2} d^{-1}$. Overall, BR and CR rates were higher in the open ocean stations than in the coastal
435 ones with highest rates (> 1 and $> 2.5 \mu\text{mol C L}^{-1} d^{-1}$, respectively) in the top 60 m (Fig. 5b; SI
436 Fig. S4a). Integrated BP, in contrast, was generally higher at the coastal stations with 5.6-10.8
437 mmol C $m^{-2} d^{-1}$ compared to the open ocean ones with 1.4-8.2 mmol C $m^{-2} d^{-1}$ (Table 1).
438 However, volumetric BP rates were not significantly different from the open ocean (Tukey
439 $p > 0.05$), where BP rates were more variable. At the coastal stations, the highest BP rates were
440 observed either at the surface (5 m) or at around ~ 40 m depth, while in the open ocean, the
441 highest rates were constantly found in the surface samples (Fig. 5c). BGE was determined for
442 the upper 50 m and showed little variability with depth (Table 2; Fig. 5d). However, BGE was
443 significantly higher (Tukey, $p < 0.05$) at the coastal stations ($9.6 \pm 3.7\%$ to $14.1 \pm 1.7\%$)
444 compared to the open ocean ones (1.7 ± 0.1 to $4.2 \pm 0.04\%$). We estimated the predominance
445 of autotrophy/heterotrophy in the system, by dividing the PP_{TOT} rates by CR (Mouriño-
446 Carballido and McGillicuddy 2006). Heterotrophic conditions ($\frac{PP_{TOT}}{CR} < 1$) occurred at the open
447 ocean stations throughout the water column, while autotrophic conditions ($\frac{PP_{TOT}}{CR} > 1$) prevailed
448 at the coastal St. E5 ($\frac{PP_{TOT}}{CR}$ ratio ranging from 0.7 to 1.9; Table 2). This pattern was preserved
449 when data were integrated over the mixed layer (Fig. 6). PP_{DOC} rates were sufficient to satisfy
450 the BCD at the coastal St. E5, but not in the open ocean stations (Table 2).

451 In the CE and at the Frontal Zone, integrated heterotrophic bacterial abundance ranged from
452 8.2-23.7 $\times 10^{15}$ cells m^{-2} (Table 1). In the CE, substantial variation of bacterial abundance
453 occurred within the upper 20 m (Fig. 5a), with an abundance of $< 1 \times 10^9$ cells L^{-1} in the western
454 periphery of the CE and $> 3 \times 10^9$ cells L^{-1} in the CE core stations. Depth-integrated BR and CR
455 ranged between 59.1 and 320 and between 135 and 592 mmol C $m^{-2} d^{-1}$, respectively (Table 1).

456 Elevated BR and CR rates (> 1 and $2.5 \mu\text{mol C L}^{-1} \text{d}^{-1}$, respectively) were only present in the
457 upper ~30-40 m of the CE (Fig. **5b**; SI Fig. **S4a**). Integrated BP rates ranged from 5.6 to 36.7
458 $\text{mmol C m}^{-2} \text{d}^{-1}$ in the CE and at the Frontal Zone stations (Table **1**). BP rates were elevated in
459 the upper 40 m of the CE and at the Frontal Zone, and significantly higher than in the majority
460 of the coastal and open ocean stations (Tukey $p < 0.05$). Stations in the core of the CE had BGEs
461 (Table **2**; Fig. **5d**) significantly higher than at the stations located in the open ocean (Tukey,
462 $p < 0.05$). BGE had a range of 2.7 ± 2.9 to $18.3 \pm 1.0 \%$ and 5.1 ± 0.2 to $5.5 \pm 2.4\%$ in the CE
463 and the Frontal Zone stations, respectively. Highest BGE was observed at 15 m depth in the CE
464 core (18.3%, St. EDM-4E). The CE and Frontal Zone stations showed net hetero- as well as net
465 autotrophy (Table **2**), with a $\frac{\text{PP}_{\text{TOT}}}{\text{CR}}$ ratio ranging from 0.2 to 1.9. When integrated over the mixed
466 layer (Fig. **6**), stations within the core of the CE and at the Frontal Zone were net autotrophic,
467 with a $\frac{\text{PP}_{\text{TOT}}}{\text{CR}}$ ratio ranging from 1.42 to 1.85, while net heterotrophy occurred at the eddy
468 periphery. PP_{DOC} was on average equivalent to 71% of the BCD within the CE and at the Frontal
469 Zone, ranging from 27.9 to 110% (Table **2**).



470

471 Figure 5: Depth distribution of heterotrophic bacterial abundance and activities from the surface to 100
 472 m. Heterotrophic bacterial abundance (HB; **a**), bacterial respiration (BR; **b**), bacterial production (BP;
 473 **c**), bacterial growth efficiency (BGE; **d**). Red dashed lines show the western and eastern boundary of
 474 the cyclonic eddy periphery, respectively. FZ refers to Frontal Zone. BP and CR rates at *in-situ*
 475 temperature were estimated based on López-Urrutia and Morán (2007) and on Regaudie-de-Gioux and
 476 Duarte (2012). BR rates were estimated from measured and temperature-corrected CR rates based on
 477 Aranguren-Gassis et al, (2012). Details are provided in the methods section and the SI.

478

479 Table 2: Average (mean) \pm standard deviation of microbial metabolic activities during M156: bacterial
 480 carbon demand (BCD); bacterial growth efficiency (BGE); dissolved primary production (PP_{DOC});
 481 Percentage of extracellular release (PER); total primary production (PP_{TOT}), the ratio between PP_{DOC}
 482 and BCD ($\frac{PP_{DOC}}{BCD}$) and the ratio between PP_{TOT} and CR ($\frac{PP_{TOT}}{CR}$). BCD and BGE were obtained from
 483 temperature-corrected BP and BR rates (see text). ‘-’ indicate that the parameter was not measured and
 484 ‘B.D.’ below detection (see text). Sampling date, time and depth are given in SI Table S1.

Location	Station	Depth (m)	BCD ($\mu\text{mol C L}^{-1} \text{d}^{-1}$)	BGE (%)	CR ($\mu\text{mol C L}^{-1} \text{d}^{-1}$)	PP_{DOC} ($\mu\text{mol C L}^{-1} \text{d}^{-1}$)	PER (%)	PP_{TOT} ($\mu\text{mol C L}^{-1} \text{d}^{-1}$)	$\frac{PP_{DOC}}{BCD}$ (%)	$\frac{PP_{TOT}}{CR}$
Coastal	E5	5	0.6 \pm 0.1	9.6 \pm 3.7	1.7 \pm 0.5	1.5 \pm 0.2	34.9 \pm 1.1	2.7 \pm 0.2	217.4	1.6 \pm 0.4
		20	0.5 \pm 0.1	12.2 \pm 2.6	1.3 \pm 0.4	1.2 \pm 0.1	52.6 \pm 2.7	2.5 \pm 0.1	231.4	1.9 \pm 0.4
		35	0.5 \pm 0.3	14.1 \pm 1.7	1.3 \pm 0.9	0.7 \pm 0.1	89.8 \pm 3.9	1.0 \pm 0.1	143.2	0.7 \pm 0.1
Eddy Periphery	EDZ-10N	All	-	-	-	-	-	-	-	-
	S6	All	-	-	-	-	-	-	-	-
	EDZ-8N	All	-	-	-	-	-	-	-	-
	EDZ-7N	5	3.6 \pm 0.8	6.6 \pm 0.5	7.3 \pm 1.9	-	-	-	-	-
		20	3.6 \pm 0.3	6.2 \pm 2.6	7.3 \pm 0.9	-	-	-	-	-
	EDZ-6N	All	-	-	-	-	-	-	-	-
Eddy Core	EDZ-5N	5	2.8 \pm 0.4	10.9 \pm 2.5	5.6 \pm 1.1	-	-	-	-	-
		20	1.2 \pm 0.4	16.7 \pm 3.7	2.8 \pm 1.1	-	-	-	-	-
	100	0.4 \pm 0.6	12.7 \pm 0.5	1.2 \pm 1.7	-	-	-	-	-	
		B.D.	B.D.	-	-	-	-	-	-	
EDM-4E	5	4.7 \pm 0.5	7.5 \pm 1.9	8.9 \pm 1.3	4.3 \pm 0.1	36.7 \pm 0.2	11.2 \pm 0.1	87.9	1.3 \pm 0.1	
	15	1.4 \pm 0.4	18.3 \pm 1.0	3.1 \pm 1.3	0.4 \pm 0.1	39.3 \pm 6.8	1.1 \pm 0.1	29.5	0.3 \pm 0.1	
	35	B.D.	B.D.	-	0.6 \pm 0.3	94.4 \pm 0.9	0.6 \pm 0.3	-	-	
	60	B.D.	B.D.	-	-	-	-	-	-	
EDM-3E	All	-	-	-	-	-	-	-	-	
EDM-4	5	4.8 \pm 1.1	5.9 \pm 2.7	9.3 \pm 2.9	4.3 \pm 1.0	35.1 \pm 5.7	12.6 \pm 1.2	92.3	1.4 \pm 0.4	
	23	3.6 \pm 0.2	8.1 \pm 3.5	7.1 \pm 0.7	3.9 \pm 0.2	35.7 \pm 1.4	11.0 \pm 0.3	110.0	1.5 \pm 0.4	
	40	B.D.	B.D.	-	0.3 \pm 0.1	85.3 \pm 7.1	0.3 \pm 0.1	-	-	
	100	B.D.	B.D.	-	-	-	-	-	-	
Eddy Periphery	EDM-6E	5	-	-	4.8 \pm 0.4	34.9 \pm 1.1	13.7 \pm 0.7	-	-	
		25	-	-	3.4 \pm 0.3	52.6 \pm 2.7	6.5 \pm 0.4	-	-	
		32	-	-	0.2 \pm 0.1	89.8 \pm 3.9	0.2 \pm 0.1	-	-	
	EDM-5E	All	-	-	-	-	-	-	-	
	EDM-2E	All	-	-	-	-	-	-	-	
	EDZ-4	All	-	-	-	-	-	-	-	
EDZ-3	All	-	-	-	-	-	-	-		

486 Table 2 continued:

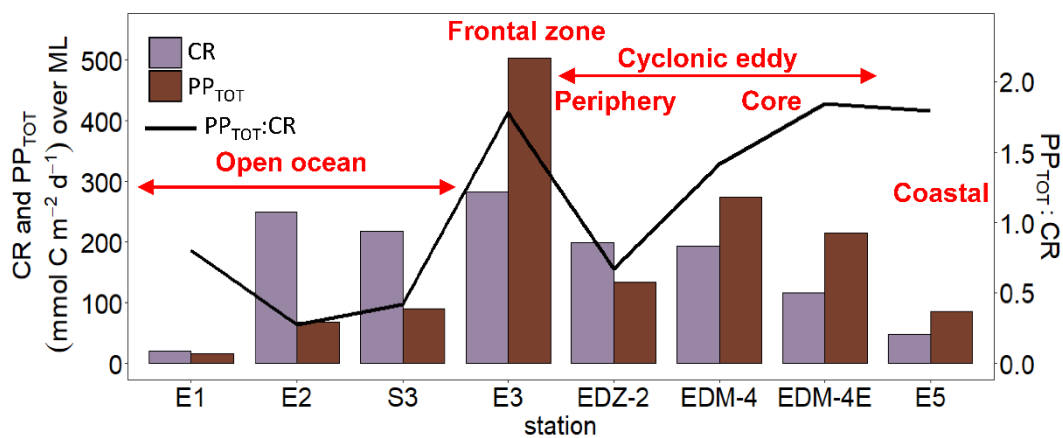
Location	Station	Depth (m)	BCD ($\mu\text{mol C L}^{-1} \text{d}^{-1}$)	BGE (%)	CR ($\mu\text{mol C L}^{-1} \text{d}^{-1}$)	PP _{DOC} ($\mu\text{mol C L}^{-1} \text{d}^{-1}$)	PER (%)	PP _{TOT} ($\mu\text{mol C L}^{-1} \text{d}^{-1}$)	$\frac{PP_{DOC}}{BCD}$ (%)	$\frac{PP_{TOT}}{CR}$	
Eddy Periphery	EDZ-2	5	10.6 ± 0.7	2.7 ± 2.9	18.2 ± 1.4	2.9 ± 0.3	25.1 ± 3.4	11.9 ± 1.0	27.9	0.7 ± 0.7	
		15	9.6 ± 2.5	4.6 ± 1.3	16.5 ± 5.3	4.9 ± 0.1	31.0 ± 1.7	14.5 ± 0.6	46.8	0.9 ± 0.1	
		50	B.D.	B.D.		0	-	-0		-	
		100	B.D.	B.D.		-	-	-		-	
Frontal Zone	E3	All	-	-		-	-	-		-	
		5	7.3 ± 0.5	5.5 ± 2.4	13.1 ± 1.3	7.8 ± 0.4	31.7 ± 1.7	25.0 ± 0.9	108.1	1.9 ± 0.7	
		25	5.0 ± 1.2	5.1 ± 0.2	9.5 ± 2.9	5.0 ± 0.6	33.4 ± 3.2	14.3 ± 0.8	96.3	1.5 ± 0.3	
		45	1.9 ± 0.7	5.4 ± 4.0	4.4 ± 1.8	0.7 ± 0.2	87.0 ± 3.3	0.8 ± 0.2	37.8	0.2 ± 0.1	
Open ocean	S4	All	-	-		-	-	-		-	
		S3	5	3.2 ± 0.6	3.0 ± 0.4	6.9 ± 1.6	1.3 ± 0.2	49.1 ± 5.5	2.7 ± 0.3	41.4	0.4 ± 0.2
			25	2.6 ± 0.5	3.1 ± 2.1	5.7 ± 1.5	1.16 ± 0.03	38.4 ± 0.9	2.5 ± 0.03	36.8	0.4 ± 0.1
			50	1.2 ± 1.1	3.3 ± 0.3	3.0 ± 2.9	0.0 ± 0.01	21.8 ± 6.6	0.1 ± 0.01	2.6	0.0 ± 0.01
	E2	100	B.D.	B.D.		-	-	-		-	
		5	1.8 ± 0.6	3.4 ± 0.4	4.3 ± 1.7	0.6 ± 0.1	40.9 ± 3.4	1.38 ± 0.1	31.4	0.3 ± 0.1	
		25	3.5 ± 1.1	1.7 ± 0.1	7.4 ± 2.9	0.94 ± 0.1	50.2 ± 3.1	1.89 ± 0.1	27.1	0.3 ± 0.1	
		50	1.7 ± 0.4	2.9 ± 0.8	4.2 ± 1.2	1.25 ± 0.3	91.3 ± 2.5	1.4 ± 0.3	72.6	0.3 ± 0.3	
	S1	100	B.D.	B.D.		-	-	-		-	
		All	-	-		-	-	-		-	
		All	-	-		-	-	-		-	
		E1	5	0.4 ± 0.3	4.2 ± 0.04	1.3 ± 0.9	0.23 ± 0.1	54.7 ± 13.3	0.39 ± 0.1	52.4	0.3 ± 0.1
25	B.D.		B.D.		0.18 ± 0.01	38.5 ± 0.6	0.43 ± 0.01		-		
75	B.D.		B.D.		0.08 ± 0.02	61.7 ± 6.2	0.13 ± 0.02		-		
125	B.D.		B.D.		-	-	-		-		

487

488

489 3.5 Semi-labile dissolved organic carbon

490 Between coastal and open ocean stations, SL-DOC concentration was not significantly different
 491 (Tukey, $p>0.05$; SI Fig. S4b) with ranges of 1.9-8.0 $\mu\text{mol L}^{-1}$ at the coastal and 1.6-18.9 μmol
 492 L^{-1} at the open ocean stations. At those sites, SL-DOC distribution was rather uniform in the
 493 upper 40 m with SL-DOC $> 5 \mu\text{mol L}^{-1}$, except from the station furthest offshore (St. E1) where
 494 SL-DOC $> 5 \mu\text{mol L}^{-1}$ was limited to shallow depths (5 m). In the CE and at the Frontal Zone,
 495 SL-DOC concentration was clearly elevated and increased from east to west with an overall
 496 range of 1.4-54.4 $\mu\text{mol L}^{-1}$. At the Frontal Zone, SL-DOC concentration $> 5 \mu\text{mol L}^{-1}$ was
 497 detectable down to 90 m depth.



498
 499
 500 Figure 6: Integrated total primary production (PP_{TOT}) and community respiration (CR) rates over the
 501 mixed layer during M156.

502
 503 3.6 Correlation analysis

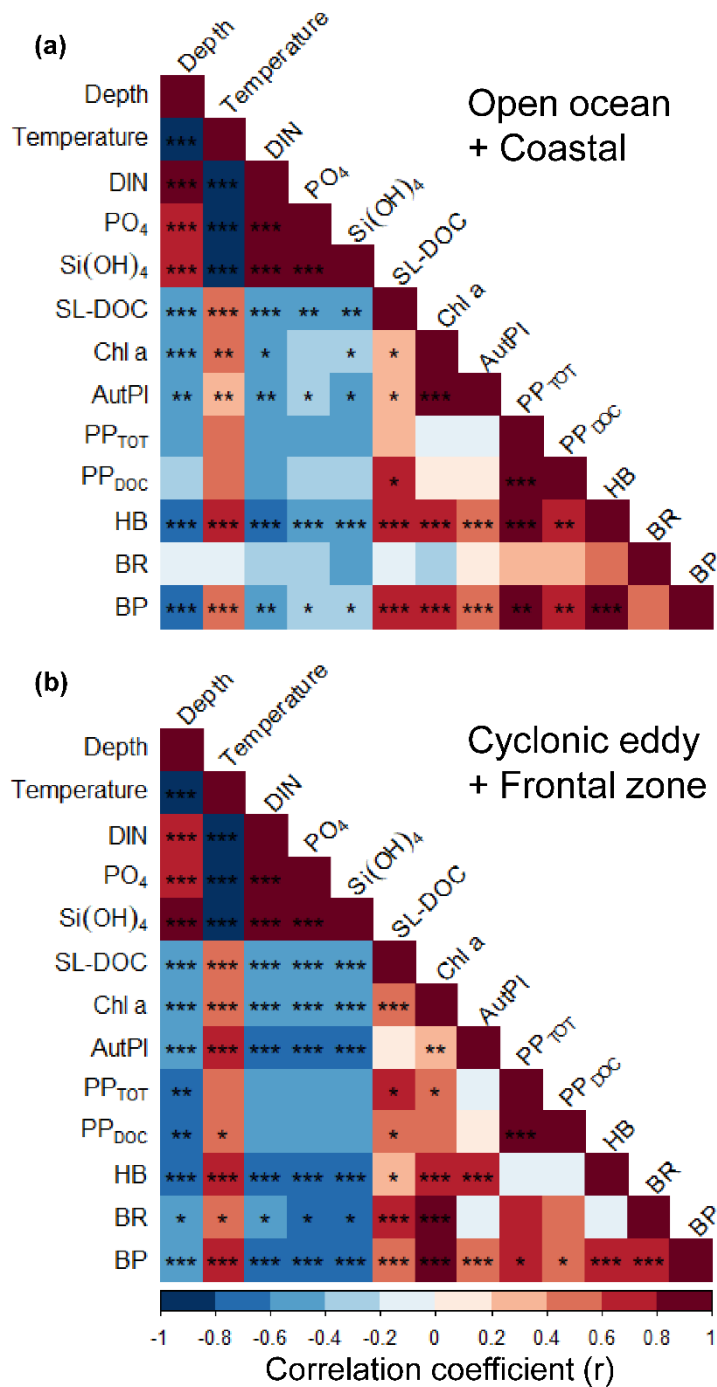
504 We applied a Pearson correlation matrix (Fig. 7) to reveal significant correlations between the
 505 measured parameters in the stations outside (open ocean + coastal) and inside (cyclonic eddy +
 506 frontal zone) the area influenced by the eddy. In both regimes, temperature correlated
 507 negatively with nutrients (DIN, PO₄, Si(OH)₄; $r = -0.70, -0.67$ and -0.67 respectively for the
 508 stations outside and $r = -0.97, -0.96$ and -0.95 for the stations inside the area influenced by the
 509 eddy, $p < 0.001$) and positively with bacterial abundances ($r = 0.51$ and 0.68 respectively,
 510 $p < 0.001$).

511 In the stations outside the influence of the eddy, total (PP_{TOT}) and dissolved primary production
 512 (PP_{DOC}) rates were not correlated to Chl-*a* or autotrophic pico- and nanoplankton biomass,
 513 $p > 0.05$). In contrast, heterotrophic bacterial abundance (HB) and the bacterial biomass

514 production (BP) were correlated to primary productivity rates ($r = 0.85$ and $r = 0.82$ respectively
515 for PP_{TOT} and $r = 0.77$ and 0.77 respectively for PP_{DOC} , $p < 0.001$), Chl-*a* ($r = 0.64$ and 0.72
516 respectively, $p < 0.001$) and autotrophic pico- and nanoplankton biomass, ($r = 0.42$ and 0.46
517 respectively, $p < 0.001$) and the concentration of semi-labile DOC (SL-DOC; $r = 0.61$ and 0.56
518, $p < 0.001$). However, bacterial respiration (BR), was not correlated to any variable ($p > 0.05$).

519 In the stations influenced by the eddy, PP_{TOT} was positively correlated to Chl-*a* ($r = 0.55$,
520 $p < 0.05$) whereas PP_{DOC} ($r = 0.47$, $p > 0.05$) was not, and both were not correlated to the
521 autotrophic pico- and nanoplankton biomass. Chl-*a* and SL-DOC were significantly correlated
522 ($r = 0.36$, $p < 0.001$). In contrast to the stations outside the eddy, HB was not correlated to PP_{TOT} ,
523 PP_{DOC} and SL-DOC ($p > 0.05$), but was still strongly correlated to Chl-*a* and autotrophic pico-
524 and nanoplankton biomass ($r = 0.57$ and 0.76 , respectively, $p < 0.001$). BP, in opposition, was
525 correlated to PP_{TOT} and PP_{DOC} ($r = 0.63$ and 0.59 , respectively, $p < 0.05$) and strongly to Chl-*a*
526 ($r = 0.92$, $p < 0.001$). BP correlated also to autotrophic pico- and nanoplankton biomass and to SL-
527 DOC, albeit to a lesser extent ($r = 0.41$ and 0.43 , respectively, $p < 0.05$). In contrast to stations
528 not influenced by the eddy, BR was strongly correlated to Chl-*a* and SL-DOC ($r = 0.83$ and 0.76 ,
529 respectively, $p < 0.001$). However, BR was not significantly correlated to autotrophic pico- and
530 nanoplankton biomass, PP_{TOT} , and PP_{DOC} ($r = -0.05$, 0.61 and 0.50 respectively, $p > 0.05$).

531



532

533 Figure 7: Pearson correlation matrix of biochemical parameters, metabolic activities, and bacterial
 534 abundance in the upper 100 m in samples not influenced by the cyclonic eddy (i.e., coastal and open
 535 ocean stations) (a) and samples influenced by the cyclonic eddy (b). Statistical significance: ‘***’<
 536 0.001, ‘**’< 0.01, ‘*’< 0.05.

537

538

4. Discussion

4.1 Effect of a cyclonic eddy on the distribution of phytoplankton abundance and activity in the Mauritanian upwelling system

In general, coastal Chl-*a* concentration during this study was not as high as observed in earlier studies with strong coastal upwelling (e.g., Alonso-Sáez et al., 2007; Agustí and Duarte, 2013; Arístegui et al., 2020). This might be related to the relatively weak upwelling resulting from weak surface winds along the Mauritanian Coast typically occurring during summer when our samples were collected (Pelegrí and Peña-Izquierdo, 2015). Consequently, during summer, fewer nutrients reach the euphotic zone. At the same time, offshore surface wind remained strong, enhanced vertical mixing and may explain why coastal Chl-*a* concentration was only slightly higher compared to the open ocean. When excluding the eddy-influenced stations, there was no marked gradient in phytoplankton productivity either, unlike other regions of the CanUS (Demarcq and Somoue, 2015; Arístegui et al., 2020). PP_{TOT} and PP_{DOC} rates stayed rather constant from the coast to the open ocean and were in the range of reported rates in oligotrophic offshore waters of the CanUS (Agustí and Duarte, 2013; Lasternas et al., 2014). Spatial distribution of SL-DOC was relatively uniform as well when considering the coastal and open ocean stations only. PER in our study was on average $51.1 \pm 17\%$ in both the open ocean and the coastal stations, which contrasts previous findings. For example, Agustí and Duarte (2013) reported PER to range from $\sim 1\%$ in ‘healthy’ communities from the upwelled waters of the CanUS to $\sim 70\%$ in ‘dying’ communities from the oligotrophic waters of the ETNA. PER have been reported to increase with nutrient depletion (Obernosterer and Herndl, 1995; Agustí and Duarte, 2013; Lasternas et al., 2014; Piontek et al., 2019) among other factors (see review by Mühlenbruch et al., 2018). Since upwelling was weak during our sampling period, low nutrient concentrations in the surface waters might explain the relatively high PER that we observed near the coast.

The CE broke this rather uniform distribution of phytoplankton productivity from the coastal to the open ocean waters. Chl-*a* isolines were pushed towards the surface in the CE (Fig. 4a). Similar uplifting of Chl-*a* isolines towards the surface has been reported for other eddies (Lochte and Pfannkuche, 1987; Feng et al., 2007; Noyon et al., 2019) and might result from phytoplankton relocation through intense vertical mixing by strong surface winds (Feng et al., 2007; Noyon et al., 2019). Before our eddy survey, strong surface winds occurred offshore (SI Fig. S5), which might explain the high Chl-*a* concentration ($>0.5 \mu\text{g L}^{-1}$) that we found at the

572 surface (5 m) of all stations within the CE. Within the eddy, we observed that Chl-*a* was higher
573 in the western than in the eastern part of the eddy (Fig. **3b** and **4a**). Chelton et al. (2011) showed
574 based on satellite observation that due to the rotational flow and the westward propagation of
575 CEs, Chl-*a* tends to accumulate in their southwest quadrants while being lower in their northeast
576 quadrants. To the best of our knowledge, this is the first time that high-resolution in situ
577 sampling could demonstrate this specific submesoscale Chl-*a* distribution within a CE. Outside
578 of the CE boundaries, we noticed a thermal front with colder surface water. Thermal fronts have
579 been detected outside of the periphery of eddies and interpreted to result from eddy-eddy
580 interaction (See review by Mahadevan, 2016) and/or eddy-wind interaction (Xu et al., 2019).
581 In this Frontal Zone, we observed higher nutrient concentrations than in the adjacent stations
582 including the western part of the CE periphery and a doming of the nutrients isolines, which
583 indicates upwelling (see Fig. **2**). Consequently, Chl-*a* was elevated, and ‘compressed’ to the
584 surface in this area similarly as in the CE (Fig. **4a**).

585 Our flow cytometry data (SI Fig. **S6**) showed that cyanobacteria (*Synechococcus*) and
586 eukaryotic pico- and nanoplankton within the CE were unevenly distributed. This suggests that
587 the phytoplankton community of the CE was likely distinct from the surrounding waters, but
588 also variable on the submesoscale within the CE. This is consistent with previous studies on
589 phytoplankton distributions in eddies (e.g., Lochte and Pfannkuche, 1987; Lasternas et al.,
590 2013; Hernández-Hernández et al., 2020). Moreover, the mixed layer was also highly variable
591 within the CE and so were PP_{TOT} rates (SI Table **S1**, Figs. **3** and **6**). We observed a three-fold
592 variation of depth-integrated PP_{TOT} rates over 100m depth (Table **1**) within the CE which is
593 coherent with earlier observations of a five-fold variation of primary production integrated over
594 the euphotic zone in a CE in the subtropical Pacific Ocean (Falkowski et al., 1991). Overall,
595 primary productivity was enhanced within the CE and the Frontal Zone with an average of four-
596 fold more depth-integrated PP_{TOT} rates over 100 m depth than in the open ocean and coastal
597 stations. This is coherent with Löscher et al. (2015), who found that depth-integrated primary
598 productivity over the Chl-*a* maximum of a CE in the Mauritanian upwelling system was three-
599 fold higher than in the surrounding waters. Extracellular release rates (PP_{DOC}) were also
600 enhanced within the eddy, but PER was slightly lower at the eddy surface (Fig. **4d, e**). We emit
601 two hypotheses regarding this distribution: 1) the lower PER was due to a higher proportion of
602 larger phytoplankton (e.g., diatoms), which have lower turnover rates and therefore lower PER
603 (Malinsky-Rushansky and Legrand, 1996) and/or 2) the upwelling of nutrients generated by the

604 CE might have enhanced the physiological health of the phytoplankton community (Agustí and
605 Duarte 2013).

606 4.2 Variations in heterotrophic bacterial abundance and activity associated with a 607 cyclonic eddy

608 Along the zonal transect, in the stations not affected by the eddy (open ocean+coastal stations),
609 a significant positive correlation was observed between HB abundance and PP_{TOT} rates (Fig.
610 7a). Those variables were rather uniformly distributed from the coast to the offshore waters
611 excluding samples influenced by the eddy, which is in agreement with earlier findings by
612 Bachmann et al. (2018) for the Mauritanian upwelling system during summer. Both our BR and
613 BP were also within the range of reported rates for coastal and offshore waters of the CanUS
614 (Reinthal et al., 2006; Alonso-Saez et al., 2007; Vaqué et al., 2014). BP rates slightly
615 decreased from the coast to the open ocean when samples from the eddy were not considered.
616 Similar trends were found in the CanUS with different upwelling intensities and during different
617 seasons (Alonso-Saez et al., 2007; Vaqué et al., 2014). The distinct distribution of BP and BR
618 rates affected the distribution of the BGE, which was higher in the coastal than in the open
619 ocean stations. Overall, our BGEs represent the lower end of global ocean values, but similarly
620 low BGEs have been observed for other EBUS, such as the CanUS (Alonso-Sáez et al., 2007)
621 the California upwelling system (del Giorgio et al., 2011) and the Humboldt upwelling system
622 (Maßmig et al., 2020). Yet, we report an average BGE two times lower than Alonso-Sáez et al.
623 (2007), which may be due to differences in upwelling intensity. Indeed, Kim et al. (2017)
624 denoted that BGE increased with increasing upwelling intensity in the Ulleung Basin. At the
625 coast, PP_{DOC} rates were sufficient to compensate for the BCD, indicating a strong trophic
626 dependence of bacteria on phytoplankton, whereas in the open ocean PP_{DOC} rates covered up
627 between 2.6 to 78% indicating a much lower trophic dependence of bacteria on phytoplankton.
628 Therefore, in the open ocean, other carbon sources (i.e., PP_{POC} , SL-DOC) must have been used
629 to compensate the BCD. SL-DOC compounds have a turnover of weeks to months, which
630 allows them to escape rapid microbial degradation (Hansell et al., 2009). Consequently, we
631 hypothesize that the BCD in the open ocean was sustained through SL-DOC produced in excess
632 near the coast and transported offshore. Indeed, in the CanUS, currents and eddies have been
633 shown to laterally transport DOC offshore up to 2000 km (Lovecchio et al., 2018).

634 Within the CE-influenced stations (CE + Frontal Zone), HB abundance was disconnected from
635 the PP_{TOT} rates (Fig. 7b). For example, in the southwestern periphery and the frontal zone HB
636 abundances were relatively low, while both PP_{TOT} rates and Chl-*a* concentrations were

637 relatively high (Fig. 4a, c). Hernández-Hernández et al. (2020) reported a similar observation
638 with a strong heterogeneity of HB biomass distribution within a CE in the CanUS. Attachment
639 to particles, viral lysis or grazing by nanoflagellates might have led to a selective reduction in
640 HB abundance. However, the exact reasons for the low HB occurrence at the eddy periphery
641 and the Frontal Zone are unknown. Despite the low HB abundance, BP was particularly
642 stimulated in these areas. On average, BP was three-fold higher in the eddy influenced stations
643 compared to the open ocean ones when integrated over 100 m. This is in accordance with earlier
644 studies from the Sargasso Sea (Ewart et al., 2008), the CanUS (Baltar et al., 2010), and the
645 Mediterranean Sea (Belkin et al., 2022), where enhanced BP has been observed in CE. As stated
646 previously, the upwelling induced by the CE and the Frontal Zone led to higher phytoplankton
647 biomass, which was likely responsible for this overall increase in BP. However, it is noteworthy
648 that BP and PP_{TOT} rates were less correlated than in the zonal transect. BR rates were also
649 enhanced at the surface of the CE and followed a similar trend as BP. SL-DOC concentrations
650 showed a strong positive correlation with BR, indicating that high molecular weight DOC
651 compounds (>1 kDa) are an available carbon source for heterotrophic microbes (Amon and
652 Benner, 1994, 1996; Benner and Amon, 2015). PP_{DOC} rates in the CE covered 27.9% to 110%
653 of the BCD, suggesting a moderate to strong trophic dependence of bacteria on phytoplankton
654 in CE. Although PP_{TOT} may satisfy the BCD in the CE (43.1-341%), a question remains about
655 why BGE was so variable and low in some parts of the CE with values down to 2.7%. One
656 explanation might be that variability of nutrient availability in the surface waters limited the
657 building of bacterial biomass (Thingstad et al., 1997; Janson et al., 2006; Berggren et al., 2010)
658 but this requires further studies.

659 Overall, we showed that autotrophy prevails in the upper 100 m depth of Mauritanian coastal
660 waters while heterotrophy prevailed offshore. This is coherent with a modeling study from
661 Lovecchio et al. (2017). The CE and the associated Frontal Zone fuelled phytoplankton nutrient
662 needs and maintained autotrophy further offshore inside of the eddy and especially in the
663 Frontal Zone, where highest PP_{TOT} were measured. Mouriño-Carballido (2009) reported from
664 indirect estimations of net community production that the frontal zones between CEs and ACEs
665 are among the most productive areas in the North-West subtropical Atlantic Ocean. Previous
666 studies have shown that the trophic balance could switch from autotrophy to heterotrophy in an
667 eddy within a month (Maixandau et al., 2005; Mouriño-Carballido and McGillicuddy, 2006).
668 Here we showed that both autotrophy and heterotrophy can occur within a single eddy. This

669 urges the need for more high-resolution eddy studies in order to better estimate their impact on
670 plankton metabolic activities and carbon cycling.

671 Conclusion

672 Our results highlight the ability of a CE to be an autotrophic vector toward the open ocean with
673 organic matter freshly produced by the phytoplankton community inside. Yet, despite the strong
674 autotrophy associated with the CE, phytoplankton exudation of DOM was not always enough
675 to compensate for bacterial metabolic needs. Even if BP was enhanced in the CE, the BGE was
676 rather low and varied substantially. Instead, heterotrophic bacteria preferentially used DOM for
677 respiration. Microbial metabolic activity dynamics within eddies are complex and require
678 further investigations to better understand and unravel carbon cycling in these features.

679

680 Data availability

681

682 All data will be made available at the PANGEA database (data manager, webmaster: Hela
683 Mehrrens)

684 Author contribution

685

686 QD, KWB and AE designed the scientific study, analyzed the data and wrote the paper. AB,
687 did the eddy reconstruction and both AB and JH commented on the paper.

688

689 Competing interests:

690

691 The authors declare that they have no conflict of interest.

692

693 Acknowledgments

694

695 We thank the captain and the crew of the *R/V Meteor* for their support during the M156 cruise.
696 We thank J. Roa, T. Klüver and L. Scheidemann for sampling on board. We thank the two
697 anonymous reviewers for their constructive comments on earlier versions of this manuscript.
698 We thank J. Roa and S. Golde additionally for the analysis of dissolved organic matter and T.

699 Klüver for cell counting, bacterial and phytoplankton activities analyses. We thank B. Domeyer
700 and R. Suhrberg for the nutrient analyses. This study has been conducted using E.U. Copernicus
701 Marine Service Information. The results contain modified Copernicus Climate Change Service
702 information 2020. Neither the European Commission nor ECMWF is responsible for any use
703 that may be made of the Copernicus information or data it contains. This study is a contribution
704 of the REEBUS project (Role of Eddies in the Carbon Pump of Eastern Boundary Upwelling
705 Systems) sub-projects WP1 and WP4, funded by the BMBF (funding reference no. 03F0815A).

706

707 Reference

708 Agustí, S., and Duarte, C. M.: Phytoplankton lysis predicts dissolved organic carbon release
709 in marine plankton communities, *Biogeosciences*, 10, 1259-1264,
710 <https://doi.org/10.5194/bg-10-1259-2013>, 2013.

711 Alonso-Sáez, L., Gasol, J. M., Arístegui, J., Vilas, J. C., Vaqué, D., Duarte, C. M., and
712 Agustí, S.: Large-scale variability in surface bacterial carbon demand and growth efficiency
713 in the subtropical northeast Atlantic Ocean, *Limnol. Oceanogr.*, 52, 533-546,
714 <https://doi.org/10.4319/lo.2007.52.2.0533>, 2007.

715 Amon, R. M. W., and Benner, R.: Rapid cycling of high molecular weight dissolved organic
716 matter in the ocean, *Nature* 369, 549–552. doi: 10.1038/369549a0, 1994.

717 Anderson, T. R., and Ducklow, H. W.: Microbial loop carbon cycling in ocean
718 environments studied using a simple steady-state model, *Aquat. Microb. Ecol.*, 26, 37-49.
719 2001.

720 Aranguren-Gassis, M., Teira, E., Serret, P., Martínez-García, S., and Fernández, E.:
721 Potential overestimation of bacterial respiration rates in oligotrophic plankton communities,
722 *Mar. Ecol. Prog. Ser.*, 453, 1–10, <https://doi.org/10.3354/meps09707>, 2012.

723 Arístegui, J., Barton, E. D., Álvarez-Salgado, X. A., Santos, A. M. P., Figueiras, F. G.,
724 Kifani, S., Hernández-León, S., Mason, E., Machú, E., and Demarcq, H.: Sub-regional
725 ecosystem variability in the Canary Current upwelling, *Prog. Oceanogr.*, 83, 33-48,
726 <https://doi.org/10.1016/j.pocean.2009.07.031>, 2009.

727 Arístegui, J., Montero, M. F., Hernández-Hernández, N., Alonso-González, I. J., Baltar, F.,
728 Calleja, M. L., and Duarte, C. M.: Variability in Water-Column Respiration and Its

729 Dependence on Organic Carbon Sources in the Canary Current Upwelling Region, *Front.*
730 *Earth Sci.*, 8, 1-12. <https://doi.org/10.3389/feart.2020.00349/>, 2020.

731 Arístegui, J., Tett, P., Hernández-Guerra, A., Basterretxea, G., Mon-tero, M. F., Wild, K.,
732 Sangrá, P., Hernández-León, S., Cantón, M., García-Braun, J. A., Pacheco, M., and Barton,
733 E. D.: The influence of island-generated eddies on Chl a distribution: a study of mesoscale
734 variation around Gran Canaria, *Deep-Sea Res.*, 44:71-96. 1997.

735 Arnon, R. M. W., and Benner, R.: Bacterial utilization of different size classes of dissolved
736 organic matter. *Limnol. Oceanogr.*, 41(1), 41–51, 1996.

737 Bachmann, J., Hassenrück, C., Gärdes, A., Iversen, M. H., Heimbach, T., Kopprio, G. A.,
738 and Grossart, H. P.: Environmental Drivers of Free-Living vs. Particle-Attached Bacterial
739 Community Composition in the Mauritania Upwelling System. *Front. Microbiol.*, 9, 1–13,
740 <https://doi.org/10.3389/fmicb.2018.02836>, 2018.

741 Baltar, F., Arístegui, J., Gasol, J. M., Lekunberri, I., and Herndl, G. J.: Mesoscale eddies:
742 Hotspots of prokaryotic activity and differential community structure in the ocean. *ISME*
743 *J.*, 4, 975-988, <https://doi.org/10.1038/ismej.2010.33>, 2010.

744 Belkin, N., Guy-haim, T., Rubin-blum, M., Lazar, A., and Sisma-, G.: Influence of cyclonic
745 and anti-cyclonic eddies on plankton biomass , activity and diversity in the southeastern
746 Mediterranean Sea. *Ocean Sci.*, 18, 693–715, <https://doi.org/10.5194/os-18-693-2022>, 1–
747 56, 2022.

748 Benner, R., and Amon, R. M. W.: The size-reactivity continuum of major bioelements in
749 the ocean. *Annu. Rev. Mar. Sci.* 7, 185–205. doi: 10.1146/annurev-marine-010213-135126,
750 (2015).

751 Berggren, M., Laudon, H., Jonsson, A., & Jansson, M. Nutrient constraints on metabolism
752 affect the temperature regulation of aquatic bacterial growth efficiency. *Microb. Ecol.*,
753 60(4), 894–902. <https://doi.org/10.1007/s00248-010-9751-1>. 2010.

754 Borchard, C. and Engel, A.: Organic matter exudation by *Emiliana huxleyi* under simulated
755 future ocean conditions, *Biogeosciences*, 9, 3405–3423, doi:10.5194/bg-9-3405-2012, 2012

756 Carlson, C. A.: Production and Removal Processes. Chapter 4 in *Biogeochemistry of*
757 *Marine Dissolved Organic Matter*, Editor(s): Hansell D. A., Carlson, C. A. AP, 805, 91–
758 151. <https://doi.org/10.1016/b978-012323841-2/50006-3>. 2002.

759 Chelton, D. B., Gaube, P., Schlax, M. G., Early, J. J., and Samelson, R. M.: The Influence
760 of Nonlinear Mesoscale Eddies on Near-Surface Oceanic Chlorophyll. *Science* 334, 328–
761 333, 2011.

762 Cheney, R. E., and Richardson, P. L.: Observed Decay of a Cyclonic Gulf Stream Ring,
763 *Deep-Sea Res. Oceanogr. Abstr.*, 23, 143-155, [https://doi.org/10.1016/S0011-](https://doi.org/10.1016/S0011-7471(76)80023-X)
764 [7471\(76\)80023-X](https://doi.org/10.1016/S0011-7471(76)80023-X), 1976.

765 Cherrier, J., Valentine, S. K., Hamill, B., Jeffrey, W. H., and Marra, J. F.: Light-mediated
766 release of dissolved organic carbon by phytoplankton. *J. Mar. Syst.*, 147: 45–51, 2015.

767 Christaki, U., Gueneugues, A., Liu, Y., Blain, S., Catala, P., Colombet, J., Debeljak, P.,
768 Jardillier, L., Irion, S., Planchon, F., Sassenhagen, I., Sime-Ngando, T., & Obernosterer, I.:
769 Seasonal microbial food web dynamics in contrasting Southern Ocean productivity regimes.
770 *Limnol. Oceanogr.*, 66(1), 108–122, <https://doi.org/10.1002/lno.11591>, 2021.

771 Couespel, D., Lévy, M., and Bopp, L.: Oceanic primary production decline halved in
772 eddy-resolving simulations of global warming, *Biogeosciences*, 18(14), 4321-4349,
773 <https://doi.org/10.5194/bg-18-4321-2021>, 2021.

774 D’Asaro, E. A.: Generation of submesoscale vortices: A new mechanism, *J. Geophys. Res.*,
775 93, 6685-6693, <https://doi.org/10.1029/JC093iC06p06685>, 1988.

776 del Giorgio, P. A., and Cole, J. J.: Bacterial Growth Efficiency in Natural Aquatic Systems.
777 *Annu. Rev. Ecol. Evol. Syst.*, 29, 503-541,
778 <https://doi.org/10.1146/annurev.ecolsys.29.1.503>, 1998.

779 Del Giorgio, P. A., Condon, R., Bouvier, T., Longnecker, K., Bouvier, C., Sherr, E., and
780 Gasol, J. M.: Coherent patterns in bacterial growth, growth efficiency, and leucine
781 metabolism along a northeastern Pacific inshore – offshore transect. *Limnol. Oceanogr.*,
782 56(1), 1–16, <https://doi.org/10.4319/lo.2011.56.1.0001>, 2011.

783 Demarcq, H. and Somoue, L.: Phytoplankton and primary productivity off Northwest
784 Africa. In: *Oceanographic and biological features in the Canary Current Large Marine*
785 *Ecosystem*. Valdés, L. and Déniz-González, I. (eds). IOC-UNESCO, Paris. IOC Technical
786 Series, No. 115, pp. 161-174. URI: <http://hdl.handle.net/1834/9186.2015>.

787 Descy, J. P., Leporcq, B., Viroux, L., François, C., and Servais, P.: Phytoplankton
788 production, exudation and bacterial reassimilation in the River Meuse (Belgium).
789 *J. Plankton Res.*, 24(3), 161-166. <https://doi.org/10.1093/plankt/24.3.161>, 2002.

790 Dickson, A. G., Sabine, C. L., and Christian, J. R.: Guide to Best Practices for Ocean CO₂
791 measurements. PICES Special Publication 3, 191 pp., 2007.

792 Dittmar, T., Cherrier, J., and Ludwighowski, K. U.: The analysis of amino acids in seawater,
793 in: Practical guidelines for the analysis of seawater, ed. by Oliver Wurl Boca Raton [u.a.],
794 CRC Press, ISBN: 978-1-4200-7306-5, 2009.

795 Dray, S.: On the number of principal components: A test of dimensionality based on
796 measurements of similarity between matrices, *Comput. Stat. Data Anal.*, 52, 4, 2228-2237,
797 2008.

798 Engel, A., Borchard, C., Piontek, J., Schulz, K. G., Riebesell, U., and Bellerby, R.: CO₂
799 increases 14C primary production in an Arctic plankton community. *Biogeosciences*, 10(3),
800 1291–1308. <https://doi.org/10.5194/bg-10-1291-2013>, 2013.

801 Engel, A., Händel, N., Wohlers, J., Lunau, M., Grossart, H. P., Sommer, U., and Riebesell,
802 U.: Effects of sea surface warming on the production and composition of dissolved organic
803 matter during phytoplankton blooms: Results from a mesocosm study, *J. Plankton Res.*,
804 33(3), 357-372, <https://doi.org/10.1093/plankt/fbq122>, 2011.

805 Engel, A., Thoms, S., Riebesell, U., Rochelle-Newall, E., and Zondervan, I.: Polysaccharide
806 aggregation as a potential sink of marine dissolved organic carbon. *Nature*, 428(6986), 929–
807 932. <https://doi.org/10.1038/nature02453>, 2004.

808 Evans, C. A., O'Reily, J. E., and Thomas, J. P.: A handbook for measurement of Chl a a
809 and primary production, College Station, TX: Texas A andM University, 1987.

810 Ewart, C. S., Meyers, M. K., Wallner, E. R., McGillicuddy, D. J., and Carlson, C. A.:
811 Microbial dynamics in cyclonic and anticyclonic mode-water eddies in the northwestern
812 Sargasso Sea, *Deep-Sea Res. II: Top. Stud. Oceanogr.*, 55(10-13), 1334-1347.
813 <https://doi.org/10.1016/j.dsr2.2008.02.013>, 2008.

814 Falkowski, P. G., Ziemann, D., Kolber, Z., and Bienfang P. K.: Role of eddy pumping in
815 enhancing primary production in the ocean, *Letters to Nature*, Vol 352, 1991.

816 Feng, M., Majewski, L. J., Fandry, C. B., and Waite, A. M.: Characteristics of two counter-
817 rotating eddies in the Leeuwin Current system off the Western Australian coast, *Deep-Sea*
818 *Res. II: Top. Stud. Oceanogr.*, 54(8-10), 961-980,
819 <https://doi.org/10.1016/j.dsr2.2006.11.022>, 2007.

820 Gargas, E.: *A Manual for Phytoplankton Primary Production Studies in the Baltic*, The
821 *Baltic Marine Biologists*, 2, 88 p., 1975.

822 Gasol, J.M., del Giorgio, P.A.: Using flow cytometry for counting natural planktonic
823 bacteria and understanding the structure of planktonic bacterial communities. *Sci. Mar.* 64,
824 197–224. 2000.

825 Gattuso J. P., Epitalon J. M., Lavigne H. and Orr J.,: seacarb: seawater carbonate chemistry,
826 R package version 3.2.13, <http://CRAN.R-project.org/package=seacarb>, 2020.

827 Grasshoff K., Kremling K., Ehrhardt M. : *Methods of sea- water analysis*. Wiley-VCH,
828 Weinheim, 1999.

829 Hansell, D. A., Carlson, C. A., Repeta, D. J., and Schlitzer, R.: Dissolved organic matter in
830 the ocean a controversy stimulates new insights. *Oceanogr.*, 22(SPL.ISS. 4), 202–211.
831 <https://doi.org/10.5670/oceanog.2009.109>, 2009.

832 Hernández-Hernández, N., Arístegui, J., Montero, M. F., Velasco-Senovilla, E., Baltar, F.,
833 Marrero-Díaz, Á., Martínez-Marrero, A., and Rodríguez-Santana, Á.: Drivers of Plankton
834 Distribution Across Mesoscale Eddies at Submesoscale Range, *Front. Mar. Sci.*, 7, 1-13.
835 <https://doi.org/10.3389/fmars.2020.00667>, 2020.

836 Ihaka R., and Gentleman R.: R: a language for data analysis and graphics. *J. Comput. Graph.*
837 *Stat.* 5, 299, 1996.

838 Jansson, M., Bergström, A. K., Lymer, D., Vrede, K., & Karlsson, J. Bacterioplankton
839 growth and nutrient use efficiencies under variable organic carbon and inorganic
840 phosphorus ratios. *Microb. Ecol.*, 52(2), 358–364. [https://doi.org/10.1007/s00248-006-](https://doi.org/10.1007/s00248-006-9013-4)
841 [9013-4](https://doi.org/10.1007/s00248-006-9013-4). 2006.

842 Jiao, N., Robinson, C., Azam, F., Thomas, H., Baltar, F., Dang, H., Hardman-Mountford,
843 N. J., Johnson, M., Kirchman, D. L., Koch, B. P., Legendre, L., Li, C., Liu, J., Luo, T., Luo,
844 Y. W., Mitra, A., Romanou, A., Tang, K., Wang, X., Zhang, R. Mechanisms of microbial

845 carbon sequestration in the ocean - Future research directions. *Biogeosciences*, 11(19),
846 5285–5306. <https://doi.org/10.5194/bg-11-5285-2014>. 2014.

847 Karstensen, J., Fiedler, B., Schütte, F., Brandt, P., Körtzinger, A., Fischer, G., Zantopp, R.,
848 Hahn, J., Visbeck, M., and Wallace, D.: Open ocean dead zones in the tropical North
849 Atlantic Ocean, *Biogeosciences*, 12, 2597-2605, <https://doi.org/10.5194/bg-12-2597-2015>,
850 2015.

851 Kelley, D. E.: *Oceanographic Analysis with R*. *Oceanographic Analysis with R*.
852 <https://doi.org/10.1007/978-1-4939-8844-0>, 2018.

853 Kim, B., Kim, S. H., Kwak, J. H., Kang, C. K., Lee, S. H., and Hyun, J. H.: Heterotrophic
854 bacterial production, respiration, and growth efficiency associated with upwelling intensity
855 in the Ulleung Basin, East Sea. *Deep Sea Res. Part II Top. Stud. Oceanogr.*, 143, 24-35,
856 <https://doi.org/10.1016/j.dsr2.2017.07.002>, 2017.

857 Kirchman, D., K'nees, E., and Hodson, R.: Leucine incorporation and its potential as a
858 measure of protein synthesis by bacteria in natural aquatic systems, *Appl. Environ.*
859 *Microbiol.*, 49(3), 599-607, <https://doi.org/10.1128/aem.49.3.599-607.1985>, 1985.

860 Lasternas, S., and Agustí, S.: The percentage of living bacterial cells related to organic
861 carbon release from senescent oceanic phytoplankton, *Biogeosciences*, 11, 6377-6387,
862 <https://doi.org/10.5194/bg-11-6377-2014>, 2014.

863 Lasternas, S., Piedeleu, M., Sangrà, P., Duarte, C. M., and Agustí, S.: Forcing of dissolved
864 organic carbon release by phytoplankton by anticyclonic mesoscale eddies in the
865 subtropical NE Atlantic Ocean. *Biogeosciences*, 10(3), 2129-2143,
866 <https://doi.org/10.5194/bg-10-2129-2013>, 2013.

867 Lathuilière, C., Echevin, V., and Lévy, M.: Seasonal and intraseasonal surface Chl a-a
868 variability along the northwest African Coast, *J. Geophys. Res. Oceans*, 113, C05007.
869 <https://doi.org/10.1029/2007JC004433>, 2008.

870 Le Vu, B., Stegner, A., Arsouze, T.: Angular momentum eddy detection and tracking
871 algorithm (AMEDA) and its application to coastal eddy formation, *J. Atmos. Oceanic*
872 *Technol.* 35, 739-762. <https://doi.org/10.1175/JTECH-D-17-0010.1>, 2018.

873 Levitus, S.: Climatological atlas of the World Ocean. NOAA Prof. Pap. 13, 1–41, 1982.

874 Lévy, M., Klein, P., and Treguier, A. M.: Impact of submesoscale physics on production
875 and subduction of phytoplankton in an oligotrophic regime, *J. Mar. Res.*, 59(4), 535-565,
876 2001.

877 Lindroth P., Mopper K.: High performance liquid chromatographic determination of
878 subpicomole amounts of amino acids by precolumn fluorescence derivatization with o-
879 phthaldialdehyde, *Anal. Chem.*, 51, 1667-1674, <https://doi:10.1021/ac50047a019>, 1979.

880 Lipson, D. A.: The complex relationship between microbial growth rate and yield and its
881 implications for ecosystem processes. *Front. Microbiol.*, 1–5.
882 <https://doi.org/10.3389/fmicb.2015.00615>. 2015.

883 Lochte, K., and Pfannkuche, O.: Cyclonic cold-core eddy in the eastern North Atlantic. II.
884 Nutrients, phytoplankton and bacterioplankton, *Mar. Ecol. Prog. Ser.*, 39, 153-164.
885 <https://doi.org/10.3354/meps039153>, 1987.

886 Lønborg, C., Martínez-García, S., Teira, E., and Álvarez-Salgado, X. A.: Bacterial carbon
887 demand and growth efficiency in a coastal upwelling system. *Aquat. Microb. Ecol.*, 63(2),
888 183–191. <https://doi.org/10.3354/ame01495>, 2011.

889 López-Urrutia, Á., and Morán, X. A. G.: Resource limitation of bacterial production distorts
890 the temperature dependence of oceanic carbon cycling, *Ecology*, 88(4), 817-822,
891 <https://doi.org/10.1890/06-1641>, 2007.

892 Löscher, C. R., Fischer, M. A., Neulinger, S. C., Fiedler, B., Philippi, M., Schütte, F., Singh,
893 A., Hauss, H., Karstensen, J., Körtzinger, A., Künzel, S., and Schmitz, R. A.: Hidden
894 biosphere in an oxygen-deficient Atlantic open-ocean eddy: Future implications of ocean
895 deoxygenation on primary production in the eastern tropical North Atlantic,
896 *Biogeosciences*, 12, 7467-7482, <https://doi.org/10.5194/bg-12-7467-2015>, 2015.

897 Lovecchio, E., Gruber, N., and Münnich, M.: Mesoscale contribution to the long-range
898 offshore transport of organic carbon from the Canary Upwelling System to the open North
899 Atlantic. *Biogeosciences*, 15(16), 5061–5091. <https://doi.org/10.5194/bg-15-5061-2018>,
900 2018.

901 Lovecchio, E., Gruber, N., Münnich, M., and Lachkar, Z.: On the long-range offshore
902 transport of organic carbon from the Canary Upwelling System to the open North Atlantic,
903 *Biogeosciences*, 14(13), <https://doi.org/10.5194/bg-14-3337-2017>, 2017.

904 Maixandeau, A., Lefevre, D., Karayanni, H., Christaki, U., VanWambeke, F., Thyssen, M.,
905 Denis, M., Fernandez, C.I., Uitz, J., Leblanc, K., Queguiner, B.: Microbial community
906 production, respiration, and structure of the microbial food web of an ecosystem in the
907 northeastern Atlantic Ocean, *J. Geophys. Res. Oceans*, 110 (C7), C07S17, 2005.

908 Malinsky-Mushansky Z. N., Legrand C. Excretion of dissolved organic carbon by
909 phytoplankton of different sizes and subsequent bacterial uptake. *Mar. Ecol. Prog. Ser.*, Vol.
910 132: 249-255, 1996. Mahadevan, A.: The Impact of Submesoscale Physics on Primary
911 Productivity of Plankton, *Annu. Rev. Mar. Sci.*, 8, 161-184,
912 <https://doi.org/10.1146/annurev-marine-010814-015912>, 2016.

913 Maßmig, M., Lüdke, J., Krahnemann, G., and Engel, A.: Bacterial degradation activity in the
914 eastern tropical South Pacific oxygen minimum zone. *Biogeosciences*, 17(1), 215–230.
915 <https://doi.org/10.5194/bg-17-215-2020>, 2020.

916 McGillicuddy Jr, D. J., Anderson, L. A., Doney S. C., and Maltrud, M. E.: Eddy-driven
917 sources and sinks of nutrients in the upper ocean: Results from a 0.1° resolution model of
918 the North Atlantic, *Glob. Biogeochem. Cycles.*, 17(2), 1035,
919 <https://doi.org/10.1029/2002GB001987>, 2003.

920 McGillicuddy, D. J.: Mechanisms of Physical-Biological-Biogeochemical Interaction at the
921 Oceanic Mesoscale, In *Annual Review of Marine Science* (Vol. 8),
922 <https://doi.org/10.1146/annurev-marine-010814-015606>, 2016.

923 Molemaker, M. J., McWilliams, J. C., and Dewar, W. K.: Submesoscale generation of
924 mesoscale anticyclones near a separation of the California Undercurrent, *J. Phys.*
925 *Oceanogr.*, 45, 613-629, <https://doi.org/10.1175/JPO-D-13-0225.1>, 2015.

926 Mouriño-Carballido, B., and McGillicuddy, D. J.: Mesoscale variability in the metabolic
927 balance of the Sargasso Sea, *Limnol. Oceanogr.*, 51(6), 2675-2689,
928 <https://doi.org/10.4319/lo.2006.51.6.2675>, 2006.

929 Mouriño-Carballido, B.: Eddy-driven pulses of respiration in the Sargasso Sea, *Deep-Sea*
930 *Res. I: Oceanogr. Res. Pap.*, 56(8), 1242-1250, <https://doi.org/10.1016/j.dsr.2009.03.001>,
931 2009.

932 Mühlenbruch, M., Grossart, H. P., Eigemann, F., and Voss, M.: Mini-review:
933 Phytoplankton-derived polysaccharides in the marine environment and their interactions

934 with heterotrophic bacteria. *Environ. Microbiol.*, 20(8), 2671–2685.
935 <https://doi.org/10.1111/1462-2920.14302>, 2018.

936 Neijssel, O. M., and Mattos, M. J. T. De.: Micro Review The energetics of bacterial growth
937 : a reassessment, *13(2)*, 179-182, 1994.

938 Nielsen, E. S.: The use of radio-active carbon (c14) for measuring organic production in the
939 sea, *ICES Mar. Sci.*, 18(2), 117-140, <https://doi.org/10.1093/icesjms/18.2.117>, 1952.

940 Noyon, M., Morris, T., Walker, D., and Huggett, J.: Plankton distribution within a young
941 cyclonic eddy off south-western Madagascar, *Deep Sea Res. Part II Top. Stud. Oceanogr.*,
942 166, 141-150, <https://doi.org/10.1016/j.dsr2.2018.11.001>, 2019.

943 Obernosterer, I., and Herndl, G. J.: Phytoplankton extracellular release and bacterial
944 growth: Dependence on the inorganic N:P ratio. *Mar. Ecol. Prog. Ser.*, 116, 247–258,
945 <https://doi.org/10.3354/meps116247>, 1995.

946 Pegliasco, C., Chaigneau, A., and Morrow, R.: Main eddy vertical structures observed in
947 the four major Eastern Boundary Upwelling Systems. *J. Geophys. Res. Oceans*, 120(9),
948 6008–6033, <https://doi.org/10.1002/2015JC010950>, 2015.

949 Pelegrí, J. L. and Peña-Izquierdo, J.: Eastern boundary currents off North-West Africa. In:
950 Oceanographic and biological features in the Canary Current Large Marine Ecosystem.
951 Valdés, L. and Déniz-González, I. (eds). IOC- UNESCO, Paris. IOC Technical Series, No.
952 115, pp. 81-92, URI: <http://hdl.handle.net/1834/9179>, 2015

953 Piontek, J., Endres, S., Le Moigne, F. A. C., Schartau, M., and Engel, A.: Relevance of
954 Nutrient-Limited Phytoplankton Production and Its Bacterial Remineralization for Carbon
955 and Oxygen Fluxes in the Baltic Sea. *Front. Mar. Sci.*, 6, 1–16,
956 <https://doi.org/10.3389/fmars.2019.00581>, 2019.

957 Rao, D. N., Chopra, M., Rajula, G. R., Durgadevi, D. S. L., and Sarma, V. V. S. S.: Release
958 of significant fraction of primary production as dissolved organic carbon in the Bay of
959 Bengal, *Deep Sea Res. Part I Oceanogr. Res.*, 168, 1-27,
960 <https://doi.org/10.1016/j.dsr.2020.103445>, 2021.

961 Regaudie-De-Gioux, A., and Duarte, C. M.: Temperature dependence of planktonic
962 metabolism in the ocean. *Glob. Biogeochem. Cycles*, 26(1), GB1015,
963 <https://doi.org/10.1029/2010GB003907>, 2012.

964 Reinthaler, T., Bakker, K., Manuels, R., van Ooijen, J., and Herndl, G. J.: Erratum to Fully
965 automated spectrophotometric approach to determine oxygen concentrations in seawater
966 via continuous-flow analysis. *Limnol. Oceanogr. Methods* 5(1), 72–72.
967 <https://doi.org/10.4319/lom.2007.5.72>, 2006.

968 Robinson C.: Heterotrophic bacterial respiration. In: Kirchman DL (ed) *Microbial ecology*
969 *of the oceans*, Wiley-Liss, New York, NY., 2008.

970 Russell, J. B. and Cook, M. G.: *Energetics of Bacterial Growth : Balance of Anabolic and*
971 *Catabolic Reactions*, *Microbiol Rev.*, 59(1), 48-62, 1995.

972 Schlitzer, R.: *Ocean Data View*, odv.awi.de, 2020.

973 Schütte, F., Brandt, P., and Karstensen, J.: Occurrence and characteristics of mesoscale
974 eddies in the tropical northeastern Atlantic Ocean, *Ocean Sci.*, 12, 663-685,
975 <https://doi.org/10.5194/os-12-663-2016>, 2016.

976 Simon, M., and Azam, F.: Protein content and protein synthesis rates of planktonic marine
977 bacteria, *Mar. Ecol. Prog. Ser.*, 51, 201-213, 1989.

978 Singh, A., Gandhi, N., Ramesh, R., and Prakash, S.: Role of cyclonic eddy in enhancing
979 primary and new production in the Bay of Bengal, *J. Sea Res.*, 97, 5-13,
980 <https://doi.org/10.1016/j.seares.2014.12.002>, 2015.

981 Smith, D., and Azam, F.: A simple, economical method for measuring bacterial protein
982 synthesis rates in seawater using. *Mar. Microb. Food Webs*, 6(2), 107-114, 1992.

983 Solórzano, L.: Determination of Ammonia in Natural Waters by the Phenolhypochlorite
984 Method, *Limnol. Oceanogr.*, 14, 799-801, 1969.

985 Strickland, J.D.H. and Parsons, T.R.: *A Practical Handbook of Seawater Analysis*. Bulletin
986 of Fisheries Research Board of Canada, 167, 1-311, 1968.

987 Thingstad, T. F., Hagström, Å., and Rassoulzadegan, F.: Accumulation of degradable DOC
988 in surface waters: Is it caused by a malfunctioning microbial loop? *Limnol. Oceanogr.*,
989 42(2), 398–404. <https://doi.org/10.4319/lo.1997.42.2.0398>. 1997.

990 Thomsen, S.: The formation of a subsurface anticyclonic eddy in the Peru-Chile
991 Undercurrent and its impact on the near-coastal salinity, oxygen, and nutrient distributions,
992 *J. Geophys. Res. Oceans*, 121, 476-501, <https://doi.org/10.1002/2015JC010878>, 2016.

993 Vaqué, D., Alonso-Sáez, L., Aristegui, J., Agustí, S., Duarte, C. M., Montserrat Sala, M.,
994 Vázquez-Domínguez, E., and Gasol, J. M.: Bacterial production and losses to predators
995 along an Open ocean productivity gradient in the Subtropical North East Atlantic Ocean. *J.*
996 *Plankton Res.*, 36(1), 198-213, <https://doi.org/10.1093/plankt/fbt085>, 2014.

997 Wear, E. K., Carlson, C. A., and Church, M. J.: Bacterioplankton metabolism of
998 phytoplankton lysates across a cyclone-anticyclone eddy dipole impacts the cycling of
999 semi-labile organic matter in the photic zone, *Limnol. Oceanogr.*, 65(7), 1608-1622,
1000 <https://doi.org/10.1002/lno.11409>, 2020.

1001 Wickham H.: tidyverse: Easily Install and Load ‘Tidyverse’ Packages. See [https://cran.r-](https://cran.r-project.org/package=tidyverse)
1002 [project.org/package=tidyverse](https://cran.r-project.org/package=tidyverse), 2016.

1003 Wilhelm, W. L.: Die Bestimmung des im Wasser gelösten Sauer- stoffes, *Ber. Dtsch. Chem.*
1004 *Ges.*, 21, 2843-2854, 1888.

1005 Xu, G., Dong, C., Liu, Y., Gaube, P., and Yang, J.: Chl a Rings around Ocean Eddies in the
1006 North Pacific, *Sci. Rep.*, 9(1), 1-8, <https://doi.org/10.1038/s41598-018-38457-8>, 2019.